Overlapping stimulons arising in response to divergent stresses in *Escherichia coli*

Huijing Wang[1,†,*],

GW McElfresh[1,‡,*],

Nishantha Wijesuriya[2],

Adam Podgorny[1],

Andrew D. Hecht[2,§],

J. Christian J. Ray[1,2,¶,‡,#]

[*]Equal contribution.

[†]Present address:

University of Pittsburgh, School of Medicine
Department of Computational and Systems Biology
3501 Fifth Avenue
10051-7A Biomedical Science Tower 3
Pittsburgh, PA 15260 USA

[‡]Present address:

Oregon National Primate Research Center
Oregon Health and Science University
Beaverton, OR 97006 USA

[#]Present address:

Inscripta
5500 Central Avenue
Boulder, CO 80301 USA

[¶]Corresponding author.

Research conducted at the following address:

[1]Center for Computational Biology
[2]Department of Molecular Biosciences
University of Kansas
2030 Becker Dr.
Lawrence, KS 66047
USA


Email: christian.ray@inscripta.com

Abstract

Cellular responses to stress can cause a similar change in some facets of fitness even if the stresses are different. Lactose as a sole carbon source for *Escherichia coli* is an established example: too little causes starvation while excessive lactose import causes toxicity as a side-effect. In an *E. coli* strain that is robust to osmotic and ionic differences in growth media, B REL606, the rate of antibiotic-tolerant persister formation is elevated in both starvation-inducing and toxicity-inducing concentrations of lactose in comparison to less stressful intermediate concentrations. Such similarities between starvation and toxification raise the question of how much the global stress response stimulon differs between them. We hypothesized that a common stress response is conserved between the two conditions, but that a previously shown threshold driving growth rate heterogeneity in a lactose-toxifying medium would reveal that the growing fraction of cells in that medium to be missing key stress responses that curb growth. To test this, we performed RNA-seq in three representative conditions for differential expression analysis. In comparison to nominally unstressed cultures, both stress conditions showed global shifts in gene expression, with informative similarities and differences. Functional analysis of pathways, gene ontology terms, and clusters of orthogonal groups revealed signatures of overflow metabolism, membrane component shifts, and altered cytosolic and periplasmic contents in toxified cultures. Starving cultures showed an increased tendency toward stringent response-like regulatory signatures. Along with other emerging evidence, our results show multiple possible pathways to stress responses, persistence, and possibly other phenotypes. These results suggest a set of overlapping responses that drives emergence of stress-tolerant phenotypes in diverse conditions.

1. Introduction

Fitness and survival of a single-celled species across diverse environments incur classic trade-offs between metabolic costs and improvement of survival probability: an effective response in one environment may incur penalties in another. Mesophilic bacteria have adapted to life in intermediate conditions where several dimensions of the cellular environment can readily cause stress, such as excessively high or low temperatures, acidity, nutrients, osmotic pressure, chemical concentrations, and so on. In the lifecycle of an enteric bacterium, drastic changes arise within and between the host and *in natura* conditions.

One such stress is antibiotics. The widespread use of antibiotics to treat livestock for enhanced meat production as well as the rise of antibiotic-resistant bacterial strains in medical contexts lends the question practical importance. Genetic resistance may also have an important relationship with transient antibiotic
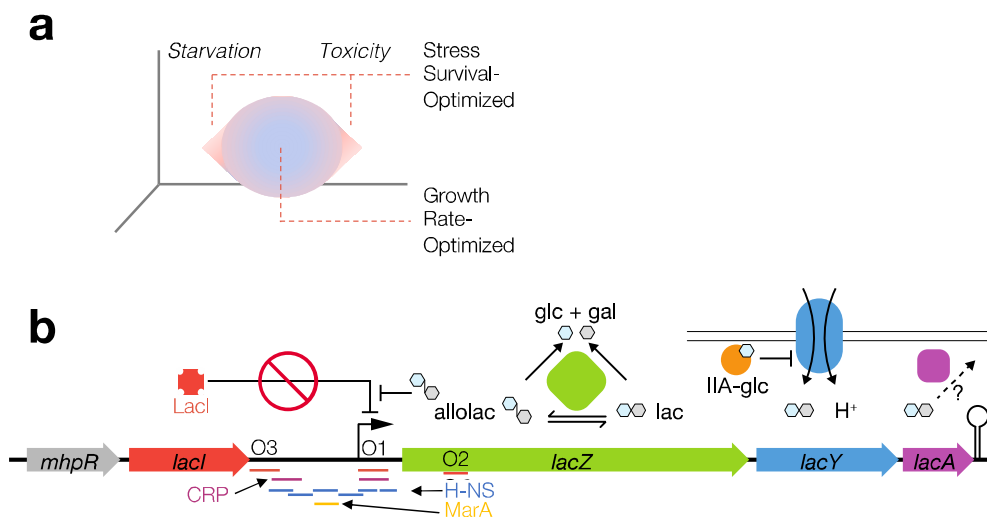
tolerance: persistence may allow resistance to evolve more quickly (3, 4), though this hypothesis has been contested. Multiple mechanisms induce persister formation (5-9), including starvation or loss of metabolic activity (10-14).

We previously demonstrated that excessively high or low lactose concentrations (as a sole carbon source) can predispose populations of bacteria derived from a strain of *Escherichia coli*, B REL606, to lowered death rates in antibiotics (15). Varying the concentration of lactose in a minimal medium drives a non-monotonic relationship with the exponential growth rate in culture, with a fast-growth plateau at intermediate concentrations (15). Lactose has established toxic effects on *E. coli* cultures, often attributed to membrane depolarization via excessive proton symport with lactose through the permease LacY, a member of the major facilitator superfamily of permeases (16-18). In B REL606, toxic lactose levels create a heterogeneous population dynamic with a chance of fast-growing cells to enter growth arrest, yet both starving and toxified cultures exhibit increased stress tolerance (15, 19; Fig. 2). Growth-arrested cells represent a persister-prone subpopulation in both conditions such that the toxified culture has the effect of a bet-hedging dynamic with average population growth rate sacrificed in favor of stress tolerance in a minority of the population. Does the global transcriptional program of stress responses have overall similarities between these conditions, or are key alternate pathways activated? The mechanisms for these conflicting stresses to attain a similar phenotype are unknown.

We interrogated this system with the bulk (population-level) RNA-seq under the hypothesis that a common stress response is conserved between starvation and toxicity. While making use of bioinformatic, biochemical, and physiological data about specific mechanisms, we avoided presuming that any particular mechanism was at work beyond the proven phenomena arising in these culture conditions. We cultured *E. coli* in low, intermediate, and high concentrations of lactose minimal medium, grew them to mid-exponential phase, and harvested biomass from each culture for bulk RNA-seq. The resulting transcriptional profiles were subjected to differential expression analysis with the intermediate lactose concentration as the reference condition.
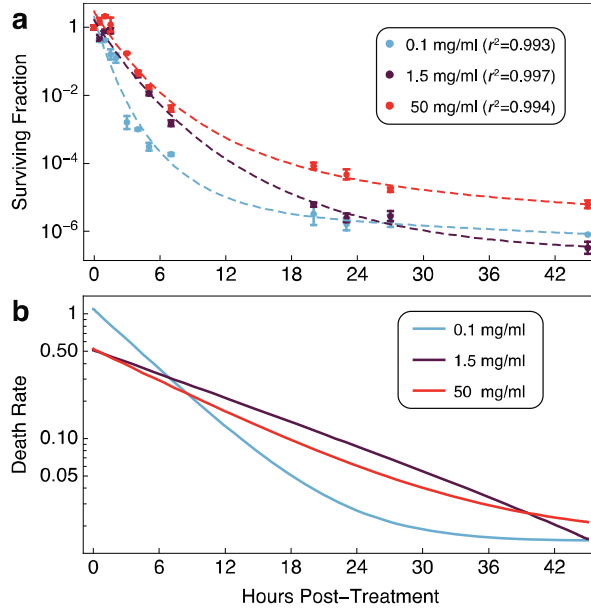
Figure 2. The killing rate of an *E. coli* B strain in ampicillin is lowest in starving and toxified culture conditions. **a.** Surviving fractions in low, intermediate, and high lactose conditions after ampicillin treatment (100 mg/ml) during mid-exponential phase (mean $\pm$ standard deviation, $N = 3$; final point in 1.5 mg/ml, $N = 1$). Data from (2) were fit to a mixed linear-exponential model $y = a\,t + b\,e^{-g\,t} + c$ with r^2 as reported in the figure. **b.** Time derivative $-\frac{dy}{dt}$ of the statistical model parameterized for each fit in panel **a** shows a lowered killing rate for both starving and toxified cultures between approximately 7 and 40 hours post-treatment. Model fit parameters:

$(\text{dose}): (a, b, c, g)$

$(0.1): (-0.0149675, 5.71624, -5.40263, 0.189278)$

$(1.5): (0.00427562, 7.13623, -6.91445, 0.072367)$

$(50): (-0.0161676, 4.99618, -4.53027, 0.101607)$

2. Results

2.1. Slowed killing rate in starving and toxified E. coli cultures

Re-analysis of our previously measured timecourse of exponential-phase *E. coli* treat-

ed with ampicillin demonstrates a lowered rate of death in starving and toxified cultures (Fig. 2). To confirm this, we fitted the data to a mixed linear-exponential statistical model in logarithmic coordinates on the y axis: $y = a\,t + b\,e^{-g\,t} + c$. All three parameters were fit with low error ($r^2 > 0.99$). Taking the time derivative of the statistical model revealed the estimated rate of killing for each culture condition (Fig. 2b): highest in non-stressful conditions. Thus, both the starving and toxified cultures are prone to produce higher levels of antibiotic tolerance than less stressful intermediate conditions.

2.2. Differential gene expression analysis reveals growth-mediated shifts in lac operon expression, toxin-antitoxin responses, and global regulator responses

To analyze gene expression profiles, we purified total RNA from early-mid-exponential cell culture in different lactose concentrations. We mapped sequencing reads to the reference genome *E. coli* B REL606 NC_012967.1 (20) with kallisto (21) and subsequently analyzed the count data using DESeq2 in R (22) with subsequent processing in Python. Setting the moderate lactose concentration (2.5 mg/ml) condition as the reference, we defined differentially expressed genes (DEGs) in *starvation* (lactose conc. 0.1 mg/ml) and *toxified* (lactose conc. 50 mg/ml) conditions as genes with an adjusted *p*-value (false detection rate; FDR) of below 0.05 and a $\log_2$ fold change (LFC) greater than 1 (Figure 3).
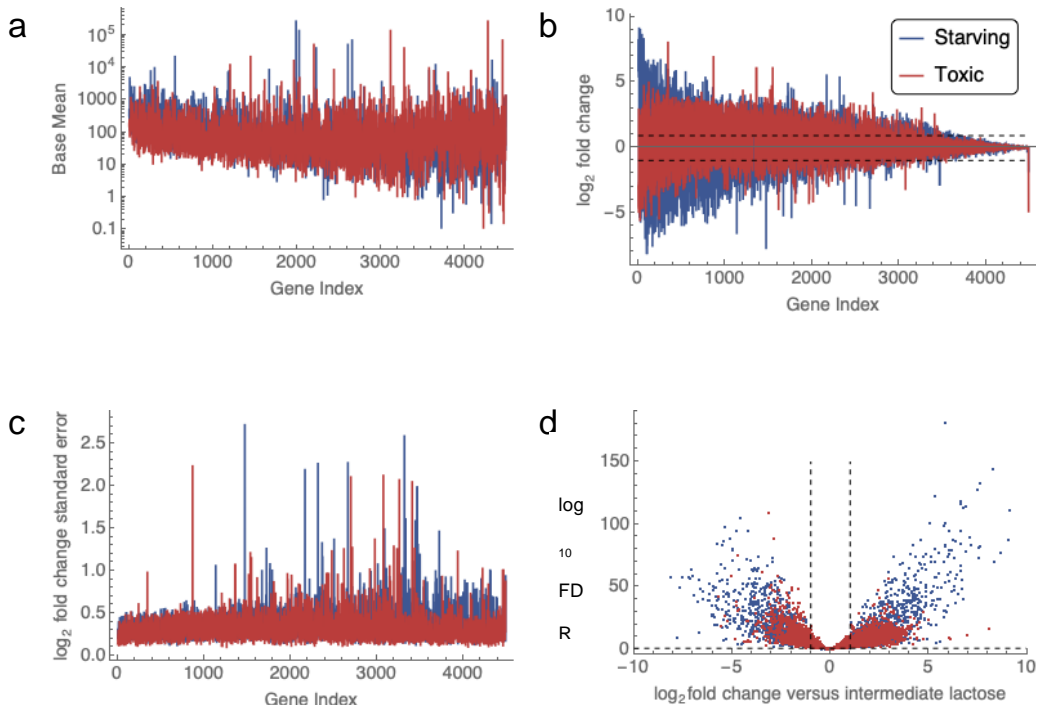
Figure 3. Comparison of differential expression profiles between starving and toxified cultures, both relative to a nominally lower-stress condition. **a.** Base mean number of reads. **b.** Mean fold change of each gene sorted by FDR from lowest to highest (Gene Index). Dashed lines indicate > 2-fold change in expression compared to intermediate-lactose cultures. **c.** Standard error of the fold change mean between biological replicates. N = 7 biological replicates for starving cultures, 9 for toxified cultures, and 9 for intermediate lactose cultures. **d.** Volcano plot reveals the extent of differential expression. Dashed lines indicate thresholds for meeting the criterion for significant differential expression: > 2-fold change and false detection rate (FDR) < 0.05.

In Figure 3a, the base mean is the normalized mean expression level for each gene in all replicates in the culture condition. The standard errors from the shrunken $\log_2$ fold change to corresponding maximum-likelihood estimates are well controlled (Figure 3c). They aligned well for a proper size factor calculation. Overlaying the differential expression $\log_2$ fold change shows that the starving cultures had wider $\log_2$ fold changes, suggesting a more extensive regulon, and perhaps more severe stress, compared to toxified cultures. This result is consistent with our previous results (15) and the model shown in Figure 1, where cells have a higher death rate under low lactose compared to toxic lactose conditions.

Out of 4490 genes in the genome, 1845 DEGs were upregulated and 1145 DEGs were downregulated in starvation, while 1755 DEGs were upregulated and 830 DEGs were downregulated in toxified cultures. Clustering of differentially expressed genes revealed that starving cells and toxified cultures have overlapping, but not identical, regulons (Figure 4a). Genes that were either upregulated or downregulated are color-coded points in Figure 4b. Many regulated genes trend toward equal differential expression (near the $y = x$ line), but the data reiterate here the observation that starving cultures have a larger set of gene
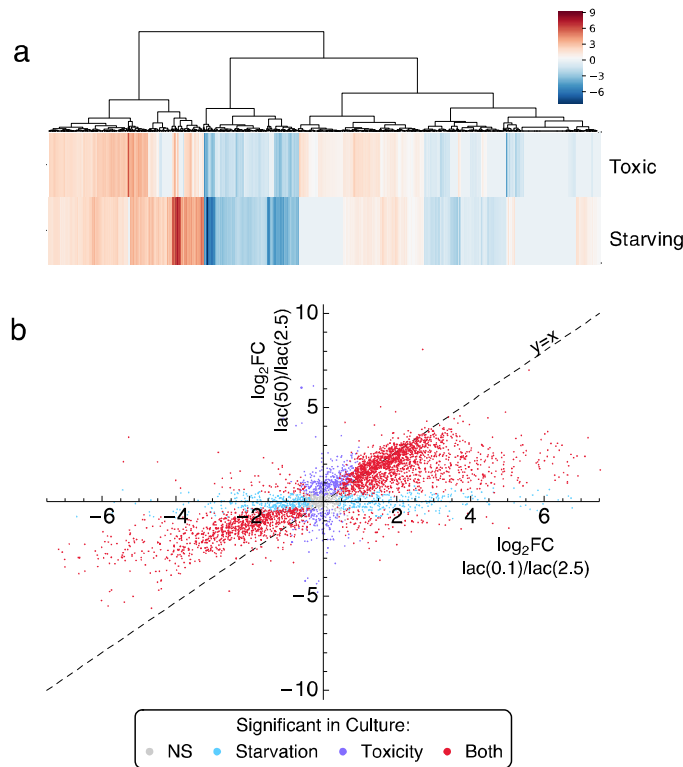
Figure 4. Fold change of genes in starving cultures versus toxified cultures relative to the intermediate baseline. **a.** DEGs clustering based on the $\log_2$ fold changes for each gene, where toxified cell profile behaves quite different from starved cells. **b.** Points are genes color-coded based on which conditions have significant fold change (FC). NS, non-significant.

expression changes than toxified cultures[1].

Expression of the *lac* operon is a natural question in experiments where the quantity of lactose in cultures is varied. The *E. coli* strain used here lacks a functional lactose regulator (LacI), an intentional choice to disentangle the downstream consequences of lactose processing without the added complication of *lac* operon gene regulation. Because the *lacI* gene has a point mutation, detected transcripts encoding LacI were non-functional (Figure 5). Growth in lactose minimal medium requires *lac* operon expression in any case (Figure 1b). Any apparent differential expression of *lac* operon gene products is attributable to the following remaining factors (23): silencing by H-NS and MarA, activation by CRP-cAMP, σ^{70}-activated promoters, and effects on mRNA concentrations by differential loss from either growth or a shift in mRNA degradation. The particular strain we used also expresses a recombinant GFP constitutively, which we have previously exploited as an optical proxy for growth rate because slower-growing cells accumulate GFP and become brighter (15, 19).

Following the steps of lactose processing is informative to see the difference between molecular gene regulation and the consequences of fitness, growth, and selection on gene expression in culture. LacY is the lactose permease, transferring extracellular lactose across the inner membrane into the cytoplasm (Fig. 1b). The starved cells contain substantially increased expression of LacY mRNA, suggesting that surviving cells in the culture have increased lactose uptake. In toxified cultures, *lacY* is not differentially expressed, suggesting relaxed selection for high lactose permease levels. The gene *lacZ* encodes β-galactosidase, the catabolic enzyme that directly assimilates lactose into the metabolic network. *lacZ* is downregulated in toxified cultures, which may reflect the fact that most cells in the toxified culture randomly avoided toxicity by lowered lactose assimilation. Galactose degradation (the Leloir pathway) is directly downstream of lactose degradation by β-galactosidase, and UDP-galactose and galactose-phosphate

---

[1]Practical constraints prevented our study from creating a distance metric for how quantitative changes in lactose correspond to quantitative changes in gene expression beyond the cases shown here. Interpretations are thus carefully limited to categorical comparisons between the culture states rather than quantitative shifts of gene expression from changes in lactose concentration.

intermediates in the Leloir pathway can cause stress and reduce cell growth (24, 25). Differential expression of *lacA* has unclear functional consequences and may simply reflect co-expression with *lacZ* and *lacY* from the operon.

We next explored differential expression of global regulators of growth rate: toxin-antitoxin systems (Fig. 5b) and transcriptional regulators (Fig. 5c). With gene annotation matching (see Methods), we found a total of 15 toxin-antitoxin (TA) modules existing in the B REL606 strain of *E. coli*. Among these TA modules, starving cultures exhibited activation of 6, including *ygiT-mqsR*, YhfG-Fic, Xre-HipA, *yeeUV*, *ghoTS* and *hokE-lexA*. Interestingly, *ygiT-mqsR*, *yeeUV*, and *ghoTS* are also upregulated in toxified cultures, while the other 3 TA systems show upregulated toxin genes. Knockouts of the global regulators in Fig. 5c result in at least a 10-fold decrease in persister formation (26). In starving cultures, 6 global regulators out of 9 are downregulated, including stress response regulator genes *dnaKJ*, DNA protection-related regulator genes *hupAB*, a folate-dependent enzyme inhibitor gene *ygfA*, and persister cell formation regulator gene *yigB*. Though the recombination-related regulator genes *ihfAB* are upregulated, suggesting a possible higher mutation rate, *dksA* is also upregulated; the latter's product can promote DNA recombination repair (27). The product of *dksA* is also an rRNA repressor that mediates stress responses and inhibits DnaK. Thus, we observe a pattern of gene regulation with counterbalancing effects that may be consistent with phenotypic decisions being made post-translationally. In toxified cultures, *ihfB* and the chemotaxis signaling genes *cheZ* and *cheY* were upregulated.
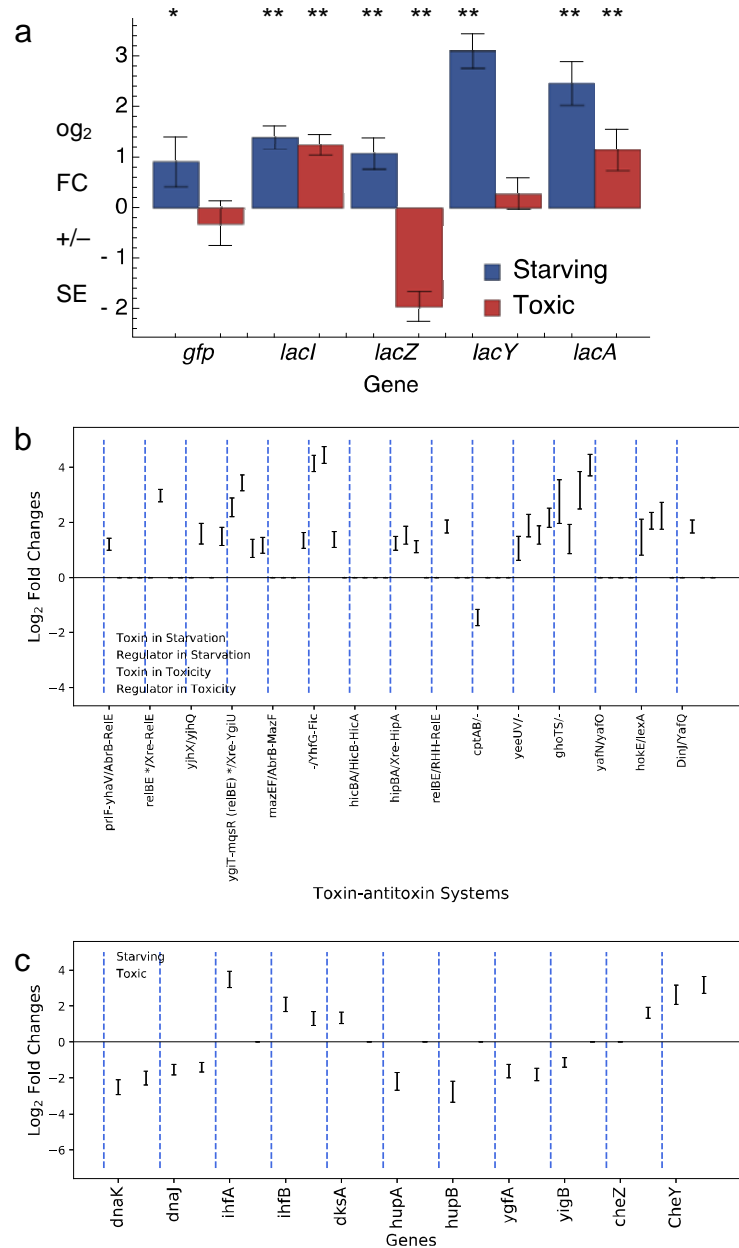
Figure 5. Differential expression $\log_2$ fold changes of reference genes in starving and toxified cultures establishes a baseline reference for persister-prone conditions. **a.** lactose operon activities. In this strain, the *lacI* gene is present but non-functional because of a mutation. As a result, the *lac* operon is expressed constitutively, as is the inserted *gfp* gene. FC, fold change. SEM, standard error of the mean. N = 7 for starving cultures, 8 for toxified cultures, and 8 for intermediate lactose cultures. **: FDR < 0.001; *: FDR < 0.05. **b.** Toxin-antitoxin systems. **c.** Global regulator genes and chemotaxis signal transduction related genes (*cheZ* and *cheY*).

2.3 Stress responses regulated by sigma factors

Transcription initiation for *E. coli* promoters requires sigma (σ) factors, subunits of RNA polymerase (RNAP) (28), making them global regulators of responsiveness to the environment. Individual promoters typically respond to specific σ factors. Six σ factors are known in *E. coli* B REL606. σ^{28} (RpoF/FliA), the flagellar synthesis sigma factor in *E. coli* strain K-12 MG1655, is missing in REL606 and σ^{19} (FecI), the ferric citrate sigma factor regulating iron transport and metabolism, is present but does not have any anno-tated gene regulatory roles in RegulonDB (29). To understand how σ factors regulate cellular responses to environmental stimuli, we explored their differential expression between lactose concentrations and that of their regulated genes as $\log_2$ fold changes (LFC2).
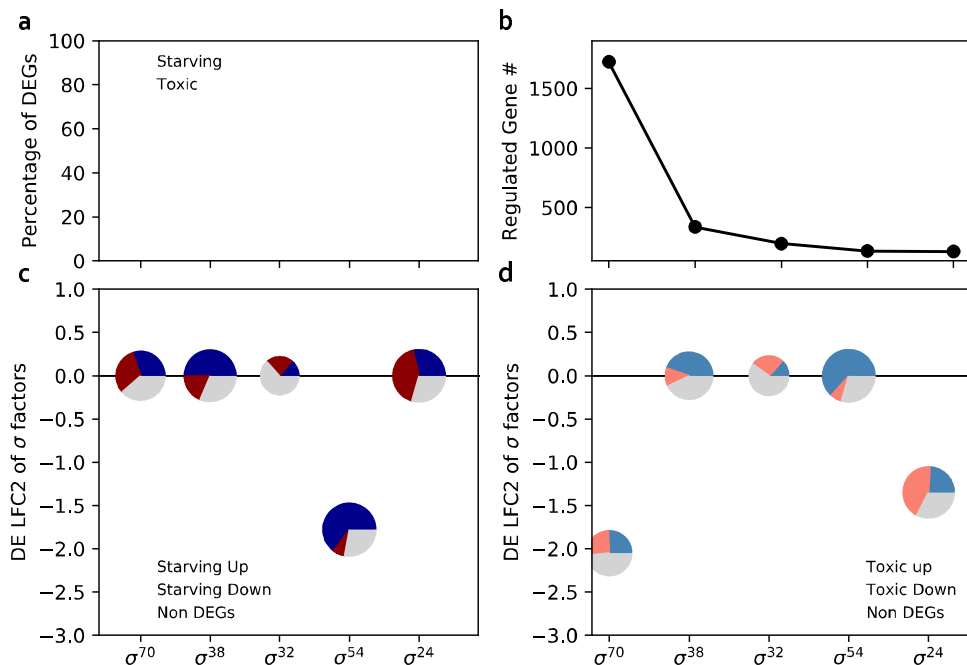
ferentially expressed genes (DEGs) in each σ factor regulon. **b.** The number (#) of genes annotated to be regulated by each σ factor. **c, d.** Differential expression ($\log_2$ fold change) of the σ factors and their regulons in **c.** starving and **d.** toxified cultures. The size of the pie chart reflects the DEG percentage regulated by each sigma factor. LFC2, $\log_2$ fold change.

Our results show a significant decrease in σ^{70} (*rpoD*) in toxified, but not starving, cultures (Fig. 6c,d). This σ factor initiates transcription in a set of approximately 1723 genes involving cell proliferation-

related behavior such as substrate uptake, DNA replication, membrane synthesis, and ribosome production (23). About half of the genes initiated by σ^{70} were downregulated in both toxified and starving conditions, suggesting an overlapping regulon between the stress responses in starved and toxified cultures.

σ^{38} (rpoS), the sigma factor associated with the stringent response, does not appear to be differentially expressed on average in starving or toxified cultures, yet a plurality of genes regulated by σ^{38} is upregulated in both conditions as compared to growth-optimized lactose concentrations. This observation is consistent with σ^{38} regulation arising from sigma factor competition, especially in toxified cultures. The ratio of σ^{70} to σ^{38} in toxified cultures is consistent with this model as well. (p)ppGpp is involved in both production and activity of σ^{38} (30). The (p)ppGpp synthases, *relA* and *spoT*, are downregulated in both starving and toxified cultures. This is not necessarily inconsistent with the presence of the stringent response, as (p)ppGpp is known to exhibit a transient increase early in the stringent response, possibly before we sampled the cultures for RNA-seq (31).

σ^{54} (rpoN) stimulates transcription initiation in 136 genes involving nutrient limitation such as nitrogen assimilation, substrate-specific transport systems, and utilization of alternative carbon and energy sources. Most genes in the σ^{54} regulon are downregulated in both starving and toxified cultures, despite σ^{54} itself being downregulated or not significantly differentially expressed in starving and toxified cultures. The best-characterized mechanism for σ^{54} interactions with σ^{38} is through the glutamate-dependent acid resistance (GDAR) system (*gadE, gadA, gadBC*) (32). σ^{54} is described as a repressor for GDAR system, while σ^{38} is annotated as an activator.

σ^{24}, driving responses to heat shock and other stresses on the membrane and periplasmic proteins, is downregulated on average in toxified cultures but is not significantly regulated in starvation here. σ^{24} is required for transcription of *degP*, a gene coding for a protease that degrades abnormal proteins in the periplasm (33). Downregulation of σ^{24} may result in less DegP protease, causing accumulation of DegP targets. Such accumulation is associated with increased membrane resilience, which is relevant because

one of the factors thought to stabilize this strain of *E. coli* in toxified cultures is resistance to osmotic stress caused by excessive lactose import (see Discussion).

In all, downregulation of σ^{70} may drive a stimulon associated with σ^{38}- and σ^{54}-compatible promoters. The majority of genes regulated by σ^{38} and σ^{54} encode stress responses in both nutrient scarcity and conditions of over-abundance. However, sigma factor $\log_2$ fold changes are not always consistent with the dominant trend of gene differential expression, which we interpret to mean that post-translational interactions drive part of the response and that additional regulatory factors play a role in the responses of *E. coli* to starving and toxified conditions.

As starvation and toxicity are both intertwined with metabolism, we performed metabolic pathway gene set enrichment analysis in peripheral (Section 2.4) and central (Section 2.5) metabolism. We used the normalized enrichment score (NES), a statistic that reflects the degree that a pathway is overrepresented at the top or bottom of a ranked list of genes (Methods Section 4.5). An overview of our pathway enrichment analysis is presented in Figure S2.

2.4 Peripheral metabolic pathway gene set enrichment analysis

2.4.1 Pathway regulatory similarities between starving and toxified cultures

Gene set enrichment analysis calculates trends for defined gene sets. The similarity of pathway regulation was calculated using rank correlations (Spearman's ρ) with differential gene expression profiles (see Methods Section 4.5.1).

Figure S3 shows the correlation between pathway regulation in starvation and toxicity. Each node in Figure S3 represents a pathway, with a total of 362 pathways annotated in *E. coli* B REL606. Nodes are connected by metabolite edges as annotated in EcoCyc. We found that most metabolic pathways are either similarly regulated or have no correlation between treatments. We observed conserved regulatory pathways for persister-prone phenotypes, including central metabolic pathways such as the pentose phosphate pathway, chorismate biosynthesis I, glycolysis I, and the superpathway of glyoxylate bypass and TCA. Glycolysis is the hub node for the pathway network with similarly regulated pathways linking to

glycolysis with degree 1 node distances. Statistically significant oppositely regulated pathways are rare.

The only oppositely regulated pathway with statistical significance is tetrahydrofolate (FH$_4$) biosynthesis, which is upregulated in starvation but downregulated in toxicity. FH$_4$ biosynthesis produces vitamin B9 (folic acid), a cofactor leading to the biosynthesis of methionine, purines, thymidylate and pantothenate.
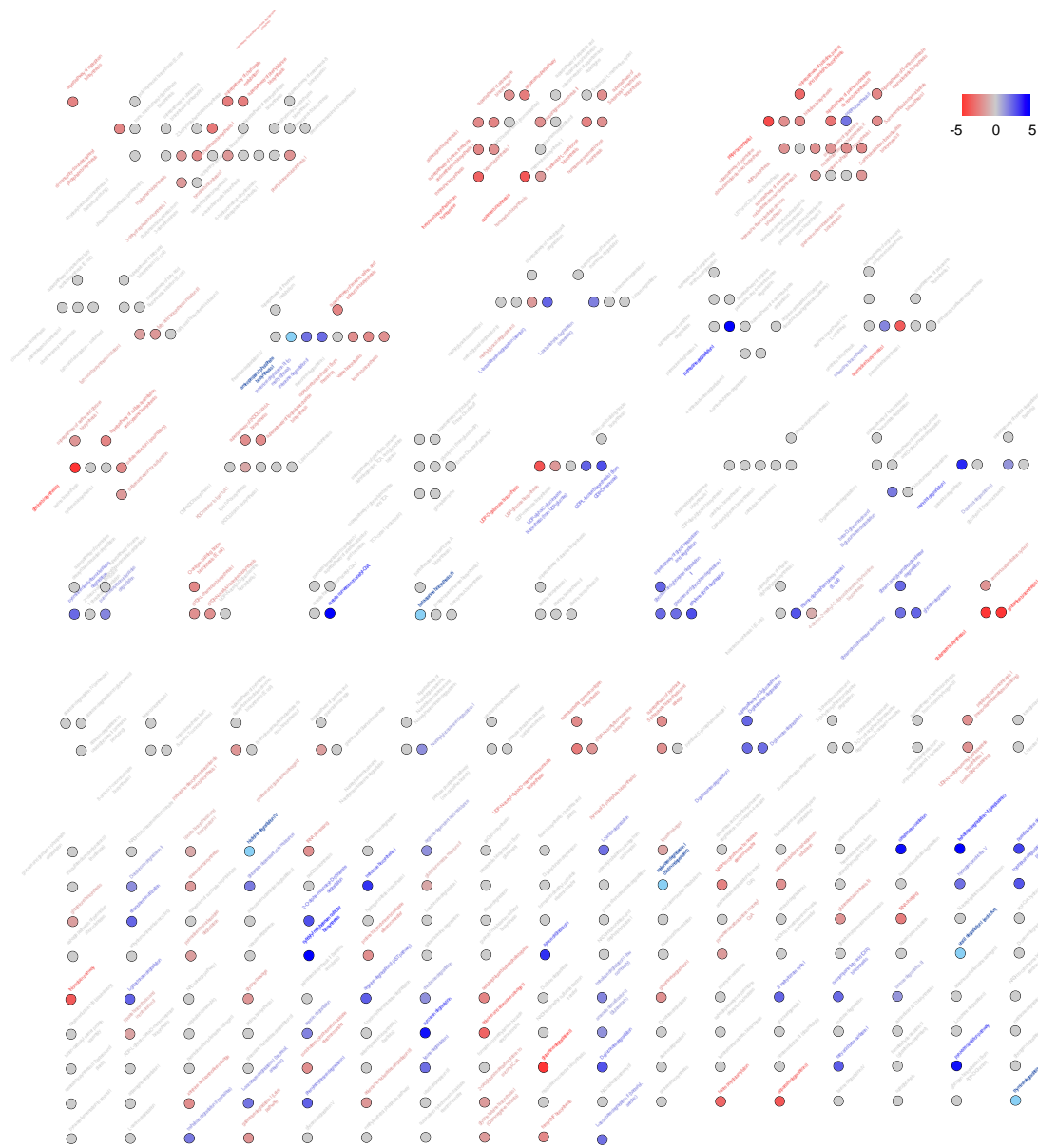
Figure 7a. Pathway enrichment score graph representation for pathway ontology in starvation condition. The upregulated pathways are shown in blue, and downregulated pathways are shown in red. The pathway ontology annotation is from EcoCyc The pathway ontology annotation is from EcoCyc (1).
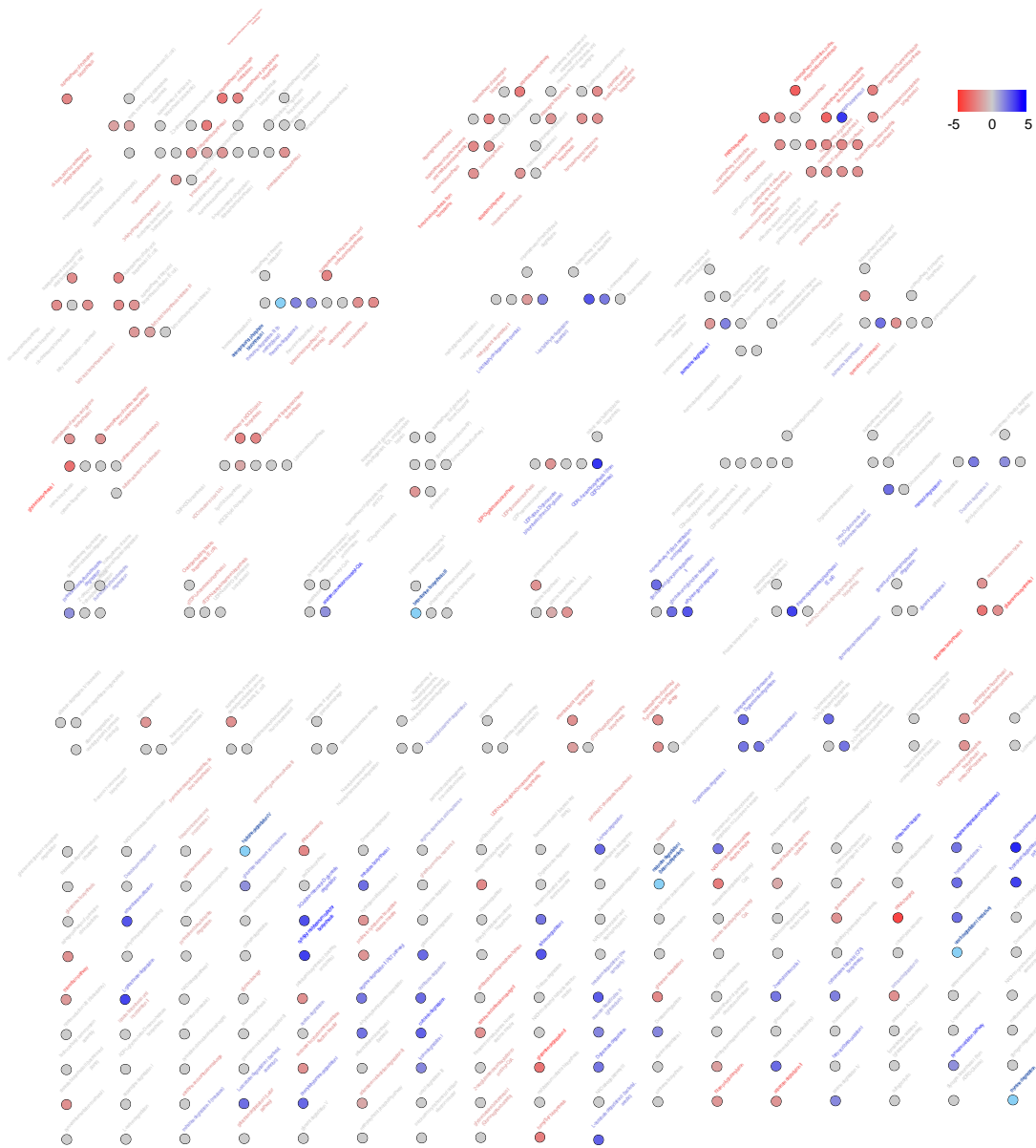
Figure 7b. Pathway enrichment analysis graph representation for pathway ontology in toxic condition. The upregulated pathways are shown in blue, and downregulated pathways are shown in red. The pathway ontology annotation is from EcoCyc (1).

2.4.2. Common enriched pathways in persister-prone phenotypes

Among 362 enriched pathways, 44 were upregulated in starvation and toxification, 69 were downregulated in starvation and toxification, 14 were uniquely upregulated in starvation, 31 pathways were uniquely downregulated in starvation, 12 pathways were uniquely upregulated in toxification, and 25 pathways were uniquely downregulated in toxification. Detailed pathway enrichment analysis results can be found in Supplementary Tables S1-S6. Figure 7 shows the pathway hierarchy structure based on EcoCyc annotations. The directed edges point to the parent pathway which is often consisted of multiple pathways to form superpathways. In Figure 7 we mapped the normalized enrichment score calculated with FGSEA (34) onto the pathway hierarchy graph. The result is many clustered enriched pathways. The top 3 clusters in Figure 7 are (1) the superpathway of chorismate metabolism, (2) amino acid biosynthesis, and (3) the superpathway of histidine, purine, and pyrimidine biosynthesis.

Chorismate is the principal precursor for the aromatic amino acids, such as tryptophan, tyrosine, and phenylalanine (35). Downregulation of chorismate biosynthesis can introduce aromatic amino acid starvation (this may occur in both toxication and starvation according to the enrichment profile). Menaquinol-8, ubiquinol-8, tetrahydrofolate biosynthesis, and enterobactin biosynthesis are not differentially regulated compared to the cultures with intermediate lactose concentration (chorismate metabolism provides essential compounds for those pathways). The quinone pool is essential for *E. coli* adapting to different oxidative conditions and maintaining proper redox- and phosphoryl-transfer reactions to form the core of cellular energetics (36). Biosynthesis of ubiquinone is reported to accumulate pathway intermediates (37, 38) with the effect of improving osmotic stress-tolerance.

We found that 17 out of 20 amino acid biosynthesis pathways are downregulated in persister-prone phenotypes accompanying upregulated amino acid degradation pathways (Table S2.). Alanine and arginine biosynthesis are uniquely downregulated in toxification, while asparagine is uniquely downregulated in starvation, implying lower NAD synthesis (39) and likely resulting in lower energy levels. Amino acid starvation can lead to accumulation of uncharged tRNAs that enter the ribosomal A site, halting transla-

tion (40). We observe downregulated tRNA charging in both toxicity and starvation. The pyrimidine, purine and pyridine nucleotide synthesis-related pathways are downregulated in both starvation and toxicity except for phosphoribosylpyrophosphate (PRPP) biosynthesis II, which provides PRPP as a pivotal metabolic precursor to pyrimidine, purine, and pyridine nucleotide synthesis. Other downregulated pathways include sulfate assimilation downstream of cysteine biosynthesis, lipid A, lipopolysaccharide (LPS) and peptidoglycan biosynthesis, spermidine biosynthesis, UDP-glucose biosynthesis, and cytochrome b_o oxidase electron transfer pathways from proline succinate.

Upregulated pathways have a sparser network structure (Table S1). Among 44 commonly upregulated pathways, 30 are degradation pathways targeting amino acids, other carbon sources, and electron transfer-related metabolites, such as L-ascorbate (vitamin C) and putrescine. Broadly upregulated nutrient assimilation pathways reflect supervening carbon source uptake and balancing energetic electron transfer. Other upregulated pathways enhance cellular fitness through energy metabolism, overflow metabolism, and membrane component regulation. In both persister-prone conditions of this study, the pyruvate oxidation pathway is upregulated; this pathway generates the transmembrane potential for constructing respiratory chains consisting of pyruvate oxidase, ubiquinone-8, and the cytochrome *bd* complex (41). Thiamine diphosphate biosynthesis I produces cofactor vitamin B1, which plays a fundamental role in energy metabolism. Trehalose pathway upregulation affects the osmotic stress response, notably present in both stress conditions. In response to acetate and osmotic pressure, the arsenate efflux pump, GDAR system, and aerobic utilization of acetate are upregulated. GDP-L-fucose biosynthesis I produces LPS components in the membrane, and membrane structure may be further stabilized by enrichment in putrescine biosynthesis III, which is the precursor for spermidine biosynthesis.

2.4.3. Uniquely enriched pathways in starvation

Pathways uniquely upregulated in starvation (Table S3) include nutrient assimilation from metabolites mannitol, D-arabinose, acetoin, glycerol, glycolate, glyoxylate, trehalose, and fatty acids. The arginine-dependent acid resistance pathway was also observed.

Though downregulation (Table S4) of the Leloir pathway may be beneficial to reduce UDP-glucose-induced toxification, it may also limit production of α-D-glucopyranose-1-phosphate, a precursor for synthesis of the outer membrane LPS component O-antigen. Despite O-antigen synthesis precursor UDP-α-D-glucuronate biosynthesis being upregulated, biosynthesis of O-antigen building blocks from precursors including α-D-glucopyranose-1-phosphate and sugars L-rhamnose, and dTDP-*N*-acetylyiosamine are specifically downregulated in starvation.

Downregulation of glutathione biosynthesis and redox reaction III may play a role in redox balance and defense against reactive oxygen species.

Several other pathways uniquely downregulated in starvation suggest a trend toward energy conservation: downregulation of lipoate metabolism, the pentose phosphate bypass, sedoheptulose bisphosphate metabolism, thiamine precursor biosynthesis, nucleotide precursor biosynthesis, and several acyl-CoA derivatives.

Finally, asparagine biosynthesis pathways are uniquely downregulated in starvation, with unclear functional significance.

2.4.4. Pathways specifically enriched in toxicity (Table S5)

Two pathways forming the *E. coli* anaerobic respiratory chain are upregulated: the formate-to-dimethyl sulfoxide electron transfer pathway and nitrate reduction III, implying increased proton-motive force across the cytoplasmic membrane (42-45). We observed upregulation of taurine degradation IV, which provides alternative sulfur under sulfate starvation induced by cysteine starvation (we note that our culture conditions are similar to those often used with this *E. coli* strain in the LTEE: Davis minimal medium containing supplemented lactose and thiamine (46) without amino acid supplementation). Several sugar degradation pathways are uniquely upregulated in toxicity, suggesting a possible carbon source alternative for *N*-acetyl-galactosamine (GalNAc), D-galactosamine (GalN), D-malate, L-rhamnose, and galactitol. Other enriched pathways are mostly fermentation metabolic pathways.

The superpathway of fatty acid biosynthesis initiation is uniquely downregulated in toxified conditions (Table S6). Related pathways such as fatty acid elongation, palmitoleate biosynthesis, and *cis*-vaccenate biosynthesis are also uniquely downregulated. Fatty acids are key building blocks for phospholipid components of cell membranes and are determinants of intracellular communication where palmitoleate is a common unsaturated fatty acid. Farnesyl pyrophosphate (FPP) biosynthesis is downregulated, possibly implying less membrane attachment in posttranslational modifications.

2.5. Gene set enrichment analysis of central metabolism

To complete the analysis of regulated metabolic pathways in starvation and toxicity, we mapped differential expression to central metabolism (Fig. 9). As the culture conditions in this study demand that the initial entry to central metabolism occurs via lactose degradation, we define central metabolism herein to be composed of the lactose degradation pathway, pentose phosphate pathway, glycolysis, Entner-Doudoroff shunt, TCA cycle, and the glyoxylate bypass. As galactose is a direct product of lactose degradation, we included the Leloir pathway (galactose degradation I) as well.

In starvation, the glycolysis pathway is mostly downregulated except for one gene encoding a phosphate transfer reaction. Components of glycolysis are more consistently upregulated in toxicity. The Entner-Doudoroff shunt linking glycolysis to the TCA cycle is regulated oppositely between starving and toxified cultures. The shunt is upregulated in starvation, possibly providing paths to alternative metabolites. Though the TCA cycle is largely downregulated in both conditions, the glyoxylate cycle is upregulated by various degrees in both starvation and toxicity. The glyoxylate cycle is a bypass for the TCA cycle to skip steps that remove CO_2, thus conserving carbon intermediates during growth (47-49). The pathway is repressed during growth on glucose, and induced by growth on acetate, the byproduct of overflow metabolism.
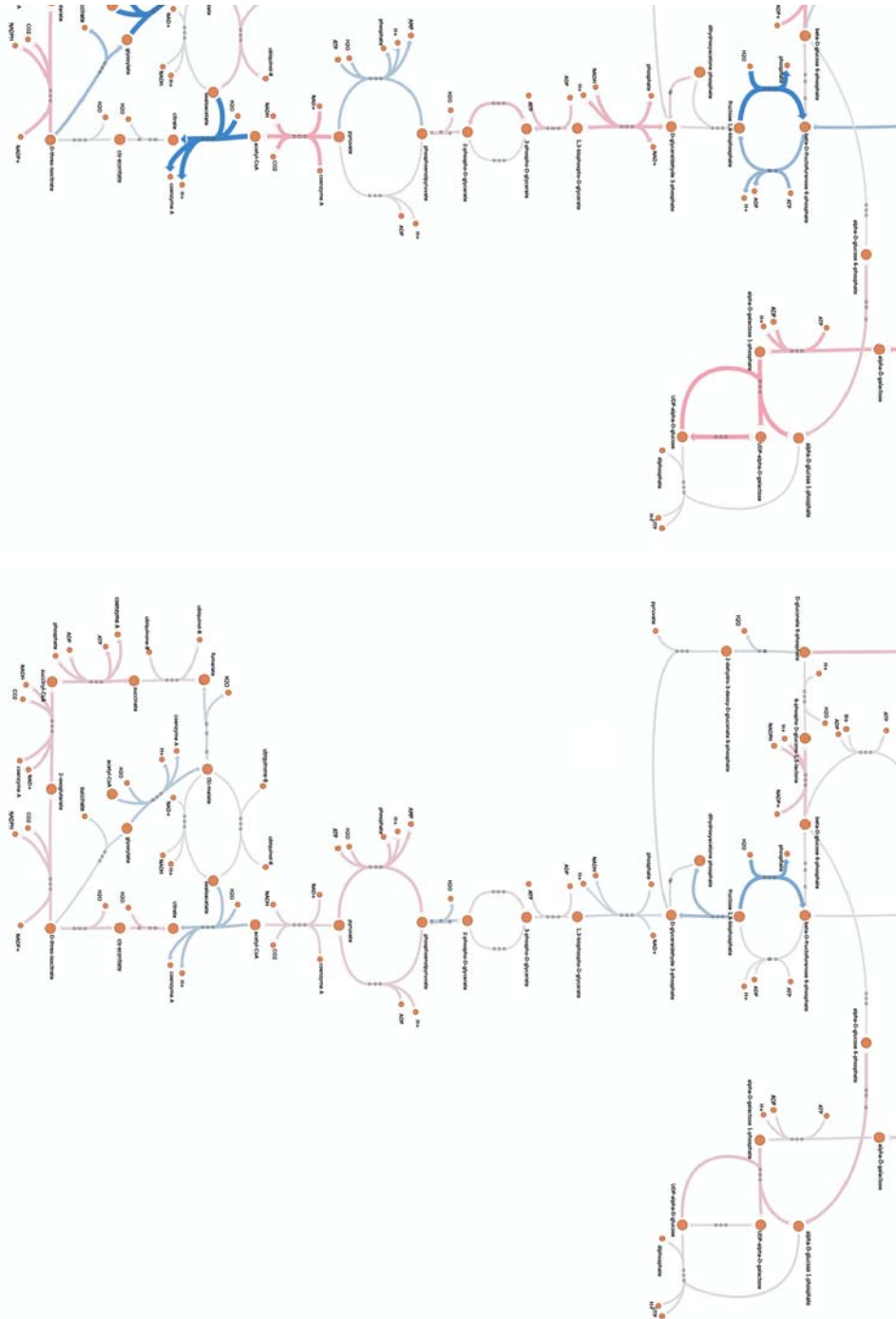
Figure 9. Differential expr

tures.

3. Discussion

Variation in fitness-relevant environmental properties affects cellular gene expression patterns in quantitative and qualitative ways. Our previous demonstration that an excess of a required nutrient drives the formation of antibiotic tolerance (15) provided an opportunity to re-evaluate the nature of integrated microbial stress responses. This phenomenon appears to arise from the robust nature of the cell wall in B strains of *E. coli*, which permits survival in adverse osmotic conditions (50). We were specifically able to enrich antibiotic-tolerant cells in conditions both below and in excess of optimal concentrations for lactose as the sole carbon source (Fig. 1). We created such conditions in batch culture to test hypotheses about the nature of antibiotic tolerance in *E. coli*: what kind of signal may predispose cells to stress tolerance, and do conditions that could be described as "opposite" of each other from osmotic, nutrient concentration, and media toxicity perspectives induce similar or largely different responses?

We conceptualized analysis of the stress response by analogy to a statistical model, with linearly independent (normalized) stress response components ξ_i and interactions ξ_{ij} between components ξ_i and ξ_j such that a given response i is independent from j if $\xi_{ij} = 0$. The integrated response can then be characterized by $\Xi = \sum_i \xi_i + \sum_{i \neq j} \xi_{ij}$ (eliding coefficients because we assume normalization between the components). The integrated response Ξ is a high-dimensional vector describing the phenotype. Independence between components may arise in some contexts and not others – we did not presume to comprehensively describe this space in our study, but rather to sample from it for exploration of the specific nature of stress responses. Nonzero interaction terms may arise from several sources, including pleiotropic effects (e.g., temperature or growth rate), co-expression (operon membership, transcriptional co-regulation, etc), and catalysis or synthesis of metabolites with broad effects (amino acids, nucleotides, tRNAs, etc).

Single cell dynamics play an important role in physiology and have a strong effect on lactose-toxified cultures. In the *E. coli* strain used in this study, a threshold drives toxicity to arrest growth in a subset of cells while subthreshold cells maintain growth. Thus, the results presented here represent an average across the subthreshold growing cells and the growth-arrested toxified subpopulation. The subthreshold

subpopulation comprises approximately 10 percent of the entire population (15). This quantity arises from exponential growth of sub-threshold cells causing them to quickly overtake the population.

We exploited extensive mechanistic knowledge about the direct effects of pathways to interpret transcriptional signatures. Targeted experiments to further test other aspects of responses, such as posttranslational effects, are beyond the scope of this study. Our results recapitulated previous interpretations of pathway analysis in stress but added crucial new results that broaden some, and narrow other, key interpretations. This study focused on the nature of the average gene expression in cultures known to be enriched for persister cells, but with no specific selection for them. In a following study, we will present an analysis of persister cells in the starving and toxified conditions that survived antibiotic treatment.

3.1. Lactose toxicity-induced persistence may arise via a combination of overflow metabolism and Leloir pathway intermediates

One hypothesis for non-starving persistence is that metabolic toxicity is induced by critical proteomic concentrations. Galactose degradation I (the Leloir pathway) is directly downstream of lactose degradation by β-galactosidase and may accumulate UDP-galactose and galactose-phosphate intermediates causing stress and loss of growth. With high metabolic rates, *E. coli* (and virtually every other species) undergoes a metabolic shift from primarily aerobic metabolism to incomplete oxidation of metabolites, including ATP synthesis (51). The cause seems to be linked to proteomic optimization, as anaerobic ATP synthesis requires a smaller fraction of the proteome to synthesize an equivalent amount of ATP at the cost of more sugar (52). The smaller proteome allows for higher growth rates due to the reduced size of the necessary metabolome, allowing more transcriptional/translational machinery to be devoted to ribosome synthesis (52, 53).

We found that toxic culture conditions that produce persister cells have apparent utilization of the Entner-Doudoroff shunt, which connects pyruvate to phosphoenolpyruvate, thus linking to the glyoxylate cycle and downregulation of the enzymes responsible for oxaloacetate and acetyl-CoA entering the citric acid cycle, consistent with cells undergoing overflow metabolism. As the only carbon source initially pre-

sent in the medium is lactose, GalE fluctuation may lead to UDP-Galactose toxicity (24), and indeed, *galE* is downregulated in high-lactose antibiotic-tolerant cells, but not significantly differentially expressed in untreated cultures.

3.2. Different phenotypes may arise from sigma factor competition

Regulation of stress responses in bacteria is generally considered to be robust to a variety of conditions. Despite being exposed to opposite stresses, we showed that differential expression of genes in starvation and toxicity is positively correlated. This may be due to leaky expression of genes in the different loci on the genome or generalized stress responses. As expected, regulated differentially expressed genes have wider fold change distributions compared to constitutively expressed genes and more genes are regulated in starvation than toxicity. We found that the global proliferation regulator σ^{70} is downregulated in toxification, potentially reducing *lac* operon expression independently of LacI. As genes regulated by σ^{38} are mostly upregulated in starving and toxified cultures, our results are consistent with the sigma factor balance leaning toward σ^{38}. The nutrient limitation-responsive sigma factor σ^{54} is downregulated in starving cells, aiding glutamate-dependent acid resistance (GDAR). In toxified conditions, downregulation of σ^{70} is drastic, moving the sigma factor competition balance towards σ^{38}. Though σ^{54} is not downregulated, GDAR is again upregulated in toxified cells. Thus, nutrient-poor and nutrient-rich conditions both stress the cells with clear regulatory responses that overlap.

3.3 Non-transcriptional and undetected factors at play in stress-responsive gene expression

Survivorship bias, as opposed to targeted transcriptional regulation, may play a role in the observed transcriptome profiles obtained from stressed cells. Noisy gene expression dynamics creates a distribution of cell states, including some in sub-optimal transcriptional states. With exponential population growth, fitter cells quickly overtake the population and dominate the measured transcriptional signal. Furthermore, it was impractical to examine every possible transcriptional function. Some that we did not emphasize, such as prophage induction, may play an uncharcterized role in distinguishing responses to di-

vergent stresses. Thus, studies of subpopulations and deeper targeted analysis may further clarify the overall similarities between divergent stresses.
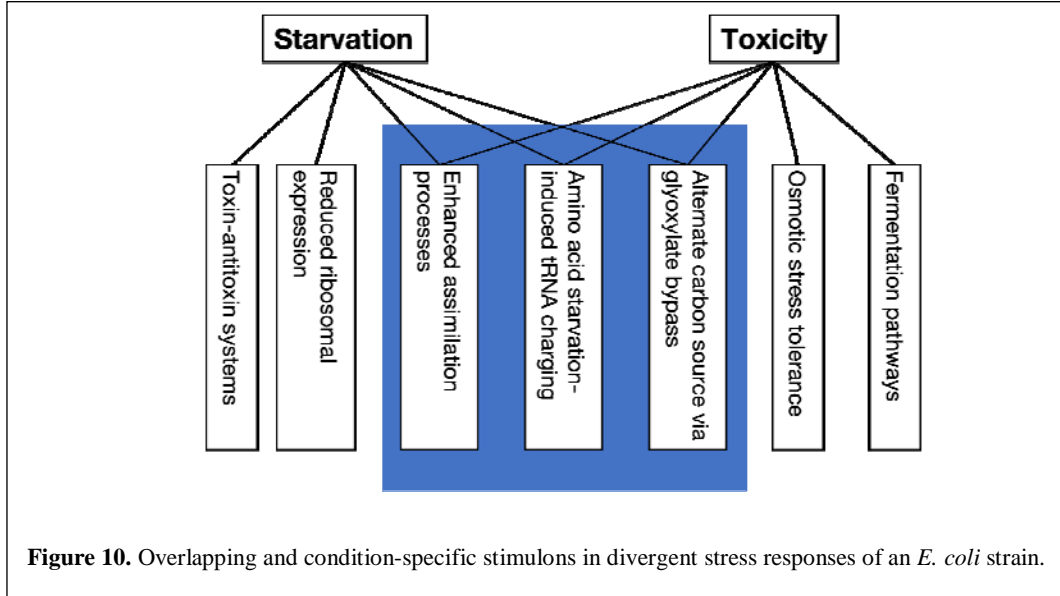
Figure 10. Overlapping and condition-specific stimulons in divergent stress responses of an *E. coli* strain.

3.4 Summary

The relationship between bacterial responses to divergent stresses contains four primary components: (*i-ii*) specific responses to each of the two stresses, (*iii*) a common stress-responsive regulon, and (*iv*) noise or functionally irrelevant responses. Overlapping responses include transcripts relating to nutrient assimilation, tRNA charging, and utilization of the glyoxylate bypass while condition-specific responses make sense in terms of unique properties of the stress in question (Fig. 10).

4. Materials and Methods

4.1. Persister Enriched RNA-Seq Experiments

E. coli B REL606 *lacI⁻* transformed with Tn7::PlacO1GFP(KanR) was inoculated in LB medium from a -80□C bacterial stock and grown for 16 hours in a 37□C shaking incubator. The LB culture was then resuspended (1:1000) into 5mL of Davis Minimal medium (DM; Difco) supplemented with thiamine and one of three lactose concentrations (0.1 mg/mL, 2.5 mg/mL, and 50 mg/mL). The cultures were allowed to acclimatize for 24 hours before being resuspended (1:1000) into 5mL of the same Davis Minimal medium and lactose concentration. Cultures were grown long enough to provide enough biomass for RNA-seq after antibiotic treatment (8 hours in 2.5 mg/mL lactose, 10 hours in 50 mg/mL lactose, and 12 hours in 0.1 mg/mL lactose). After the initial growth phase, 1.5 mL cell culture aliquots were subjected to RNA isolation according to the following procedure.

Cell cultures were pelleted in a microcentrifuge (10,000 G for 2 minutes), washed in PBS buffer twice, resuspended in 500 µL of RNA-Later (ThermoFisher) and stored in at -20□C for up to one week. RNA isolation was performed using Direct-Zol (Zymo) and TRIzol reagent (ThermoFisher) and stored in a -80□C freezer overnight. Isolated RNA was ribo-depleted using RiboZero (Illumina) with ethanol washing to precipitate the RNA. Library preparation was completed using NEBNext Ultra II Directional RNA Library Prep Kit for Illumina (New England Biolabs) and sequenced using MiSeq v3 Paired End 150 bp (Illumina). Data are available from NCBI project number PRJNA938933.

4.2. RNA-seq sequence alignment and genome annotation with Ecocyc and RegulonDB

RNA transcript quantification was performed using kallisto (21) with reference genome NC_012967.1 (20) and 10 bootstrap samples. Functional interpretations used Ecocyc (Ver. 23.1) (54) and RegulonDB (55). Lacking extensive annotation of gene regulation in REL606, we used the K-12 MG1655 strain annotation based on gene names and gene product similarities.

4.3. Differential Expression Analysis

We used R package DESeq2 (56) for gene differential expression analysis. The RNA transcription quantification data were first clustered to isolate outlier replicates using principal component analysis (PCA) (Figure S2). Two samples with a high number of missing transcripts were dropped from subsequent analysis. To confirm reproducible outcomes of sample treatment, hierarchical clustering using the Wald significance test was performed on all samples; sample treatment was retrieved perfectly (Figure S1).

The DESeq2 pipeline includes size factor estimation, dispersion estimation, and DEG tests. Low-count RNA quantifications are noisy and may decrease the sensitivity of DEGs detection (57). Size factors were calculated with a subset of control genes: non-regulated genes according to RegulonDB (55) with expression higher than a threshold (10) across all replicates. Setting transcriptome quantification from the moderate lactose condition, we applied the adaptive-T prior shrinkage estimator "apeglm" and used Wald significance tests for detecting DEGs and obtaining the $\log_2$ fold changes (LFC2).

4.4. Metabolic pathway enrichment analysis

4.4.1. Enrichment analysis by FGSEA

At the time of analysis, there were 368 pathways in EcoCyc for B REL606. 6 pathways that are not apparently regulated by gene products were discarded. Pathway enrichment was analyzed using FGSEA (58). Differentially expressed genes were pre-ranked by their $\log_2$ fold change. Pathway gene sets were defined with reference to the EcoCyc database. The pre-ranked gene data and pathway gene sets were then processed by the fgseaMultilevel function to obtain final results. Minimum gene set size was set to 3 with 200 bootstrap replicates. The threshold for pathway significance was 0.05.

Pathways in Figure 7 are linked by key metabolites and their flow direction. The pathway ontology in Figure 7 is annotated in the Ecocyc database. The pathway link and pathway ontology was extracted from EcoCyc and visualized with Cytoscape (59).

4.4.2. Pathway regulatory mechanism similarity

To calculate the similarity between pathway regulation in different conditions, we used Spearman's ρ rank correlation between the differential expression profile for each pathway. The similarity score for cases where all gene enrichment in a pathway are of the same direction is set to 1.

Metabolic pathway visualization used the Python package Escher (60).

4.5. Code availability

Analysis code is available at https://github.com/jcjray/ecoli_divergent_stress_pipeline

Acknowledgments

References

1.   Keseler IM, Mackie A, Santos-Zavaleta A, Billington R, Bonavides-Martínez C, Caspi R, Fulcher C, Gama-Castro S, Kothari A, Krummenacker M, Latendresse M, Muñiz-Rascado L, Ong Q, Paley S, Peralta-Gil M, Subhraveti P, Velázquez-Ramírez DA, Weaver D, Collado-Vides J, Paulsen I, Karp PD. The EcoCyc database: reflecting new knowledge about Escherichia coli K-12. Nucleic Acids Research. 2017;45(D1):D543-D50. doi: 10.1093/nar/gkw1003.

2.   Li C, Thio WJ-C, Sprott JC, Iu HH, Xu Y. Constructing Infinitely Many Attractors in a Programmable Chaotic Circuit. IEEE Access. 2018;6:29003-12. doi: 10.1109/ACCESS.2018.2824984.

3.   Levin-Reisman I, Ronin I, Gefen O, Braniss I, Shoresh N, Balaban NQ. Antibiotic tolerance facilitates the evolution of resistance. Science. 2017;355(6327):826-30. Epub 2017/02/12. doi: 10.1126/science.aaj2191. PubMed PMID: 28183996.

4.   El Meouche I, Dunlop MJ. Heterogeneity in efflux pump expression predisposes antibiotic-resistant cells to mutation. Science (New York, NY). 2018;362(6415):686-90. doi: 10.1126/science.aar7981. PubMed PMID: 30409883.

5.   Hofsteenge N, van Nimwegen E, Silander OK. Quantitative analysis of persister fractions suggests different mechanisms of formation among environmental isolates of *E. coli*. BMC Microbiol. 2013;13:25. Epub 2013/02/06. doi: 10.1186/1471-2180-13-25. PubMed PMID: 23379956; PMCID: PMC3682893.

6.   Tkachenko AG, Kashevarova NM, Karavaeva EA, Shumkov MS. Putrescine controls the formation of Escherichia coli persister cells tolerant to aminoglycoside netilmicin. FEMS Microbiol Lett. 2014;361(1):25-33. Epub 2014/10/07. doi: 10.1111/1574-6968.12613. PubMed PMID: 25283595.

7.   Pu Y, Zhao Z, Li Y, Zou J, Ma Q, Zhao Y, Ke Y, Zhu Y, Chen H, Baker MAB, Ge H, Sun Y, Xie XS, Bai F. Enhanced efflux activity facilitates drug tolerance in dormant bacterial cells. Mol Cell. 2016;62(2):284-94. doi: 10.1016/j.molcel.2016.03.035.

8.   Simsek E, Kim M. Power-law tail in lag time distribution underlies bacterial persistence. Proc Natl Acad Sci U S A. 2019;116(36):17635-40. Epub 2019/08/21. doi: 10.1073/pnas.1903836116. PubMed PMID: 31427535; PMCID: PMC6731627.

9.   Vega NM, Allison KR, Khalil AS, Collins JJ. Signaling-mediated bacterial persister formation. Nat Chem Biol. 2012;8(5):431-3.

10.   Cui P, Niu H, Shi W, Zhang S, Zhang W, Zhang Y. Identification of Genes Involved in Bacteriostatic Antibiotic-Induced Persister Formation. Front Microbiol. 2018;9:413. Epub 2018/03/22. doi: 10.3389/fmicb.2018.00413. PubMed PMID: 29559967; PMCID: PMC5845583.

11.   Matsumoto S, Kawai Y, Miyagawa S, Iwamoto Y, Okuda S, Sanchez-Gorostiaga A, Vicente M, Tsuneda S. Unique transcriptional profile of native persisters in Escherichia coli. J Biosci Bioeng. 2018;125(1):15-22. Epub 2017/08/20. doi: 10.1016/j.jbiosc.2017.07.015. PubMed PMID: 28821380.

12.   Harms A, Fino C, Sorensen MA, Semsey S, Gerdes K. Prophages and Growth Dynamics Confound Experimental Results with Antibiotic-Tolerant Persister Cells. MBio. 2017;8(6). Epub 2017/12/14. doi: 10.1128/mBio.01964-17. PubMed PMID: 29233898; PMCID: PMC5727415.

13. Amato SM, Orman MA, Brynildsen MP. Metabolic control of persister formation in *Escherichia coli*. Mol Cell. 2013;50(4):475-87, NIHMSID: 23665232.

14. Kwan BW, Valenta JA, Benedik MJ, Wood TK. Arrested protein synthesis increases persister-like cell formation. Antimicrob Agents Chemother. 2013;57(3):1468-73. Epub 2013/01/09. doi: 10.1128/aac.02135-12. PubMed PMID: 23295927; PMCID: PMC3591907.

15. Ray JCJ, Wickersheim ML, Jalihal AP, Adeshina YO, Cooper TF, Balázsi G. Cellular growth arrest and persistence from enzyme saturation. PLoS Comput Biol. 2016;12(3):e1004825; PMCID: PMC4820279.

16. Dykhuizen D, Hartl D. Transport by the lactose permease of *Escherichia coli* as the basis of lactose killing. J Bacteriol. 1978;135(3):876-82; PMCID: PMC222459.

17. Eames M, Kortemme T. Cost-benefit tradeoffs in engineered *lac* operons. Science. 2012;336(6083):911-5, NIHMSID: 22605776.

18. Abramson J, Iwata S, Kaback HR. Lactose permease as a paradigm for membrane transport proteins. Mol Membr Biol. 2004;21(4):227-36. PubMed PMID: citeulike:12575051.

19. Bandyopadhyay A, Wang H, Ray JCJ. Lineage space and the propensity of bacterial cells to undergo growth transitions. PLoS Comput Biol. 2018;14(8):e1006380. doi: 10.1371/journal.pcbi.1006380; PMCID: PMC6122811.

20. Pruitt KD, Tatusova T, Maglott DR. NCBI reference sequences (RefSeq): a curated non-redundant sequence database of genomes, transcripts and proteins. Nucleic Acids Res. 2007;35(Database issue):D61-5. Epub 2006/11/30. doi: 10.1093/nar/gkl842. PubMed PMID: 17130148; PMCID: PMC1716718.

21. Bray NL, Pimentel H, Melsted P, Pachter L. Near-optimal probabilistic RNA-seq quantification. Nat Biotechnol. 2016;34(5):525-7. Epub 2016/04/05. doi: 10.1038/nbt.3519. PubMed PMID: 27043002.

22. Love MI, Huber W, Anders S. Moderated estimation of fold change and dispersion for RNA-seq data with DESeq2. Genome Biology. 2014;15(12):550. doi: 10.1186/s13059-014-0550-8.

23. Karp PD, Ong WK, Paley S, Billington R, Caspi R, Fulcher C, Kothari A, Krummenacker M, Latendresse M, Midford PE, Subhraveti P, Gama-Castro S, Muniz-Rascado L, Bonavides-Martinez C, Santos-Zavaleta A, Mackie A, Collado-Vides J, Keseler IM, Paulsen I. The EcoCyc Database. EcoSal Plus. 2018;8(1). Epub 2018/11/09. doi: 10.1128/ecosalplus.ESP-0006-2018. PubMed PMID: 30406744.

24. Lee SJ, Trostel A, Le P, Harinarayanan R, Fitzgerald PC, Adhya S. Cellular stress created by intermediary metabolite imbalances. Proceedings of the National Academy of Sciences of the United States of America. 2009;106(46):19515-20. Epub 2009/11/03. doi: 10.1073/pnas.0910586106. PubMed PMID: 19887636.

25. Lee SJ, Trostel A, Adhya S. Metabolite Changes Signal Genetic Regulatory Mechanisms for Robust Cell Behavior. mBio. 2014;5(1):e00972-13. doi: 10.1128/mBio.00972-13.

26. Lewis K. Persister cells. Annu Rev Microbiol. 2010;64:357-72, NIHMSID: 20528688.

27.   Meddows TR, Savory AP, Grove JI, Moore T, Lloyd RG. RecN protein and transcription factor DksA combine to promote faithful recombinational repair of DNA double-strand breaks. Mol Microbiol. 2005;57(1):97-110. Epub 2005/06/14. doi: 10.1111/j.1365-2958.2005.04677.x. PubMed PMID: 15948952.

28.   Paget MS. Bacterial Sigma Factors and Anti-Sigma Factors: Structure, Function and Distribution. Biomolecules. 2015;5(3):1245-65. doi: 10.3390/biom5031245. PubMed PMID: 26131973.

29.   Santos-Zavaleta A, Salgado H, Gama-Castro S, Sanchez-Perez M, Gomez-Romero L, Ledezma-Tejeida D, Garcia-Sotelo JS, Alquicira-Hernandez K, Muniz-Rascado LJ, Pena-Loredo P, Ishida-Gutierrez C, Velazquez-Ramirez DA, Del Moral-Chavez V, Bonavides-Martinez C, Mendez-Cruz CF, Galagan J, Collado-Vides J. RegulonDB v 10.5: tackling challenges to unify classic and high throughput knowledge of gene regulation in E. coli K-12. Nucleic Acids Res. 2019;47(D1):D212-d20. Epub 2018/11/06. doi: 10.1093/nar/gky1077. PubMed PMID: 30395280; PMCID: PMC6324031.

30.   Nystrom T. Growth versus maintenance: a trade-off dictated by RNA polymerase availability and sigma factor competition? Mol Microbiol. 2004;54(4):855-62. Epub 2004/11/04. doi: 10.1111/j.1365-2958.2004.04342.x. PubMed PMID: 15522072.

31.   Sanchez-Vazquez P, Dewey CN, Kitten N, Ross W, Gourse RL. Genome-wide effects on Escherichia coli transcription from ppGpp binding to its two sites on RNA polymerase. Proc Natl Acad Sci U S A. 2019;116(17):8310-9. Epub 2019/04/12. doi: 10.1073/pnas.1819682116. PubMed PMID: 30971496; PMCID: PMC6486775.

32.   Riordan J, Mitra A. Regulation of Escherichia coli Pathogenesis by Alternative Sigma Factor N. EcoSal Plus. 2017. doi: doi:10.1128/ecosalplus.ESP-0016-2016.

33.   Erickson JW, Gross CA. Identification of the sigma E subunit of Escherichia coli RNA polymerase: a second alternate sigma factor involved in high-temperature gene expression. Genes Dev. 1989;3(9):1462-71. Epub 1989/09/01. doi: 10.1101/gad.3.9.1462. PubMed PMID: 2691330.

34.   Korotkevich G, Sukhov V, Budin N, Shpak B, Artyomov MN, Sergushichev A. Fast gene set enrichment analysis. bioRxiv. 2021:060012. doi: 10.1101/060012.

35.   Pittard J, Yang J. Biosynthesis of the Aromatic Amino Acids. EcoSal Plus. 2008;3(1). Epub 2008/09/01. doi: 10.1128/ecosalplus.3.6.1.8. PubMed PMID: 26443741.

36.   van Beilen JWA, Hellingwerf KJ. All Three Endogenous Quinone Species of Escherichia coli Are Involved in Controlling the Activity of the Aerobic/Anaerobic Response Regulator ArcA. Frontiers in microbiology. 2016;7:1339-. doi: 10.3389/fmicb.2016.01339. PubMed PMID: 27656164.

37.   Stefely JA, Pagliarini DJ. Biochemistry of Mitochondrial Coenzyme Q Biosynthesis. Trends Biochem Sci. 2017;42(10):824-43. Epub 2017/09/17. doi: 10.1016/j.tibs.2017.06.008. PubMed PMID: 28927698.

38.   Sévin DC, Sauer U. Ubiquinone accumulation improves osmotic-stress tolerance in Escherichia coli. Nat Chem Biol. 2014;10(4):266-72. Epub 2014/02/11. doi: 10.1038/nchembio.1437. PubMed PMID: 24509820.

39.	Begley TP, Kinsland C, Mehl RA, Osterman A, Dorrestein P. The biosynthesis of nicotinamide adenine dinucleotides in bacteria. Vitam Horm. 2001;61:103-19. Epub 2001/01/12. doi: 10.1016/s0083-6729(01)61003-3. PubMed PMID: 11153263.

40.	Haseltine WA, Block R. Synthesis of guanosine tetra- and pentaphosphate requires the presence of a codon-specific, uncharged transfer ribonucleic acid in the acceptor site of ribosomes. Proc Natl Acad Sci U S A. 1973;70(5):1564-8. Epub 1973/05/01. doi: 10.1073/pnas.70.5.1564. PubMed PMID: 4576025; PMCID: PMC433543.

41.	Koland JG, Miller MJ, Gennis RB. Reconstitution of the membrane-bound, ubiquinone-dependent pyruvate oxidase respiratory chain of Escherichia coli with the cytochrome d terminal oxidase. Biochemistry. 1984;23(3):445-53. Epub 1984/01/31. doi: 10.1021/bi00298a008. PubMed PMID: 6367818.

42.	Jones RW, Lamont A, Garland PB. The mechanism of proton translocation driven by the respiratory nitrate reductase complex of Escherichia coli. Biochem J. 1980;190(1):79-94. Epub 1980/07/15. doi: 10.1042/bj1900079. PubMed PMID: 6255943; PMCID: PMC1162066.

43.	Garland PB, Downie JA, Haddock BA. Proton translocation and the respiratory nitrate reductase of Escherichia coli. Biochem J. 1975;152(3):547-59. Epub 1975/12/01. doi: 10.1042/bj1520547. PubMed PMID: 5996; PMCID: PMC1172508.

44.	Enoch HG, Lester RL. The role of a novel cytochrome b-containing nitrate reductase and quinone in the in vitro reconstruction of formate-nitrate reductase activity of E. coli. Biochem Biophys Res Commun. 1974;61(4):1234-41. Epub 1974/12/23. doi: 10.1016/s0006-291x(74)80416-x. PubMed PMID: 4616697.

45.	Ruiz-Herrera J, DeMoss JA. Nitrate reductase complex of Escherichia coli K-12: participation of specific formate dehydrogenase and cytochrome b1 components in nitrate reduction. J Bacteriol. 1969;99(3):720-9. Epub 1969/09/01. PubMed PMID: 4905536; PMCID: PMC250087.

46.	Lenski RE. [cited 2021]. Available from: http://myxo.css.msu.edu/ecoli/dm25liquid.html.

47.	Cortay JC, Bleicher F, Duclos B, Cenatiempo Y, Gautier C, Prato JL, Cozzone AJ. Utilization of acetate in Escherichia coli: structural organization and differential expression of the ace operon. Biochimie. 1989;71(9-10):1043-9. Epub 1989/09/01. doi: 10.1016/0300-9084(89)90109-0. PubMed PMID: 2512996.

48.	LaPorte DC, Walsh K, Koshland DE, Jr. The branch point effect. Ultrasensitivity and subsensitivity to metabolic control. J Biol Chem. 1984;259(22):14068-75. Epub 1984/11/25. PubMed PMID: 6389540.

49.	Walsh K, Koshland DE, Jr. Determination of flux through the branch point of two metabolic cycles. The tricarboxylic acid cycle and the glyoxylate shunt. J Biol Chem. 1984;259(15):9646-54. Epub 1984/08/10. PubMed PMID: 6378912.

50.	Yoon SH, Han M-J, Jeong H, Lee CH, Xia X-X, Lee D-H, Shim JH, Lee SY, Oh TK, Kim JF. Comparative multi-omics systems analysis of Escherichia coli strains B and K-12. Genome Biol. 2012;13(5):R37-R. doi: 10.1186/gb-2012-13-5-r37. PubMed PMID: 22632713.

51.   Wolfe AJ. The acetate switch. Microbiol Mol Biol Rev. 2005;69(1):12-50. Epub 2005/03/10. doi: 10.1128/MMBR.69.1.12-50.2005. PubMed PMID: 15755952; PMCID: PMC1082793.

52.   Basan M, Hui S, Okano H, Zhang Z, Shen Y, Williamson JR, Hwa T. Overflow metabolism in Escherichia coli results from efficient proteome allocation. Nature. 2015;528(7580):99-104. Epub 2015/12/04. doi: 10.1038/nature15765. PubMed PMID: 26632588; PMCID: PMC4843128.

53.   Peebo K, Valgepea K, Maser A, Nahku R, Adamberg K, Vilu R. Proteome reallocation in Escherichia coli with increasing specific growth rate. Mol Biosyst. 2015;11(4):1184-93. Epub 2015/02/26. doi: 10.1039/c4mb00721b. PubMed PMID: 25712329.

54.   Keseler IM, Mackie A, Santos-Zavaleta A, Billington R, Bonavides-Martínez C, Caspi R, Fulcher C, Gama-Castro S, Kothari A, Krummenacker M, Latendresse M, Muñiz-Rascado L, Ong Q, Paley S, Peralta-Gil M, Subhraveti P, Velázquez-Ramírez DA, Weaver D, Collado-Vides J, Paulsen I, Karp PD. The EcoCyc database: reflecting new knowledge about Escherichia coli K-12. Nucleic Acids Research. 2016;45(D1):D543-D50. doi: 10.1093/nar/gkw1003.

55.   Santos-Zavaleta A, Salgado H, Gama-Castro S, Sánchez-Pérez M, Gómez-Romero L, Ledezma-Tejeida D, García-Sotelo JS, Alquicira-Hernández K, Muñiz-Rascado LJ, Peña-Loredo P, Ishida-Gutiérrez C, Velázquez-Ramírez DA, Del Moral-Chávez V, Bonavides-Martínez C, Méndez-Cruz C-F, Galagan J, Collado-Vides J. RegulonDB v 10.5: tackling challenges to unify classic and high throughput knowledge of gene regulation in E. coli K-12. Nucleic acids research. 2019;47(D1):D212-D20. doi: 10.1093/nar/gky1077. PubMed PMID: 30395280.

56.   Love MI, Huber W, Anders S. Moderated estimation of fold change and dispersion for RNA-seq data with DESeq2. Genome Biol. 2014;15(12):550. Epub 2014/12/18. doi: 10.1186/s13059-014-0550-8. PubMed PMID: 25516281; PMCID: PMC4302049.

57.   Sha Y, Phan JH, Wang MD. Effect of low-expression gene filtering on detection of differentially expressed genes in RNA-seq data. Conf Proc IEEE Eng Med Biol Soc. 2015;2015:6461-4. Epub 2016/01/07. doi: 10.1109/EMBC.2015.7319872. PubMed PMID: 26737772; PMCID: PMC4983442.

58.   Korotkevich G, Sukhov V, Sergushichev A. Fast gene set enrichment analysis. bioRxiv. 2019:060012. doi: 10.1101/060012.

59.   Shannon P, Markiel A, Ozier O, Baliga NS, Wang JT, Ramage D, Amin N, Schwikowski B, Ideker T. Cytoscape: a software environment for integrated models of biomolecular interaction networks. Genome Res. 2003;13(11):2498-504. Epub 2003/11/05. doi: 10.1101/gr.1239303. PubMed PMID: 14597658; PMCID: PMC403769.

60.   King ZA, Dräger A, Ebrahim A, Sonnenschein N, Lewis NE, Palsson BO. Escher: A Web Application for Building, Sharing, and Embedding Data-Rich Visualizations of Biological Pathways. PLOS Computational Biology. 2015;11(8):e1004321. doi: 10.1371/journal.pcbi.1004321.

Supplementary Figures
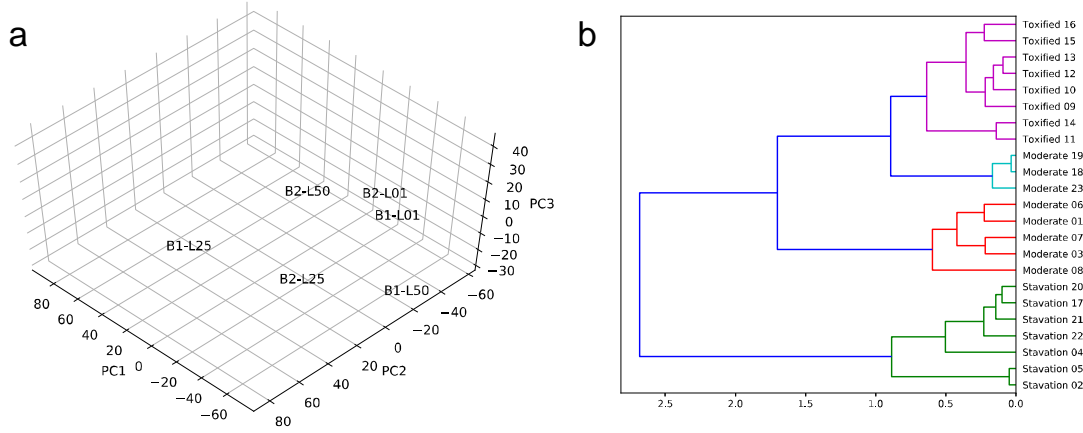
Figure S1. Data quality verification. **a**. PCA analysis for the transcriptome profile. **b**. hierarchical clustering using Wald significance. The clustering recapitulated treatment conditions.
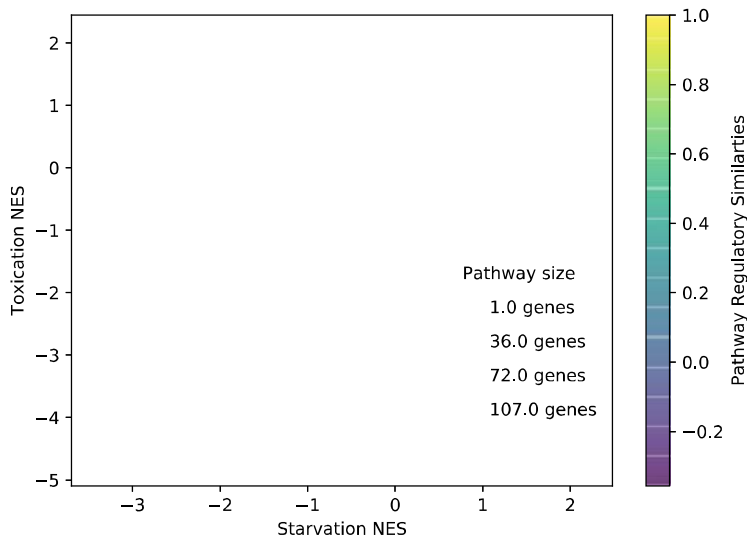
Figure S2. Pathway enrichment analysis overview. The plot is color-coded for the similarity of pathway regulation between starvation and toxicity. The size of the circle represents pathway gene set size, and the location of the bubbles are the normalized enrichment scores for each pathway.
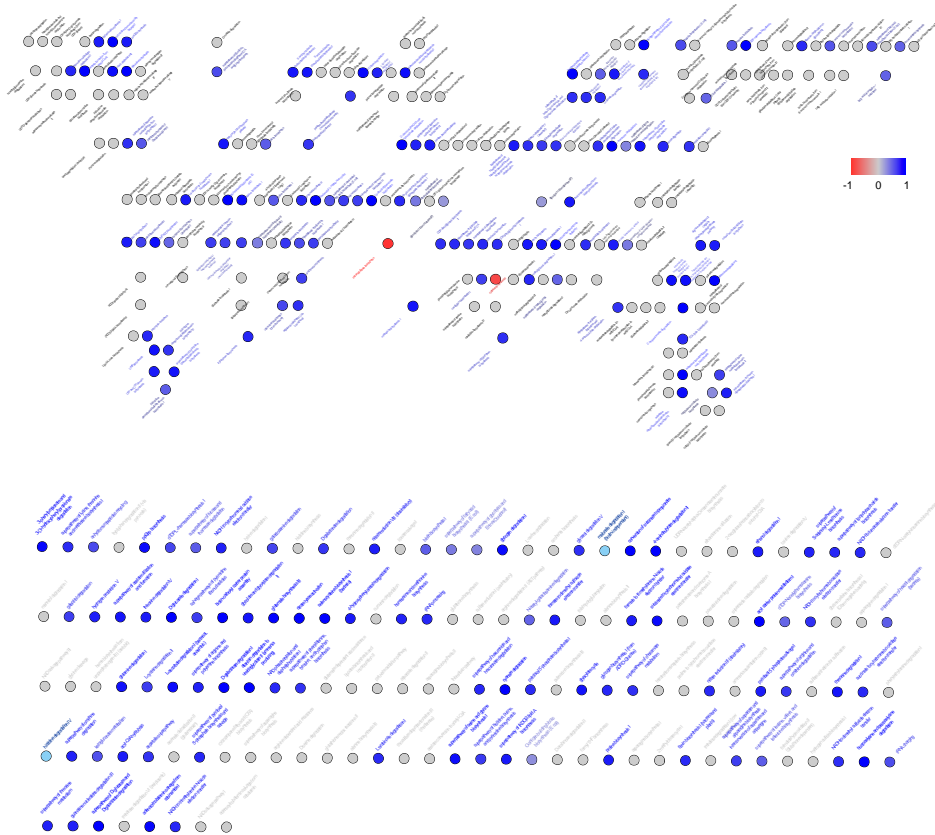
Figure S3. Pathway regulatory correlations between starving and toxified cells. Blue dots show a conserved regulatory regime for both stresses, and red dots show oppositely regulated pathways.

Supplementary Tables

Table S1. Pathways enriched in both starvation and toxification. Pathway ID and name are according to EcoCyc database annotations, and normalized enrichment score is calculated using the R package fgsea.

Pathway ID	Name	Gene Set Size	Spearman correlation	Toxication NES	Starvation NES
PUTDEG-PWY	putrescine degradation I	2	-1	1.48002492	4.65997042
PWY0-1305	glutamate dependent acid resistance	2	-1	1.1859878	1.59212915
PWY0-461	lysine degradation I	2	-1	1.35155215	1.83928035
PWY0-1317	L-lactaldehyde degradation (aerobic)	2	-1	1.46805444	2.01581953
THRDLCTCAT-PWY	threonine degradation III (to methylglyoxal)	2	-1	1.46828561	1.77182093
PWY0-1280	ethylene glycol degradation	2	-1	2.32846128	2.44590459
GLYCOLATEMET-PWY	glycolate and glyoxylate degradation I	7	0.32142857	1.88244895	1.86338914
GLYCOL-GLYOXDEG-PWY	superpathway of glycol metabolism and degradation	11	0.36446564	1.88372208	2.02611816
PWY0-42	2-methylcitrate cycle I	6	0.37142857	1.69070836	2.03799995
PWY-6961	L-ascorbate degradation II (bacterial, aerobic)	9	0.83333333	2.11098325	1.79204893
PWY-6772	hydrogen production V	7	0.85714286	1.88508666	1.77736595
PWY0-301	L-ascorbate degradation I (bacterial, anaerobic)	8	0.95238095	1.83854381	1.72700654
LYXMET-PWY	L-lyxose degradation	7	0.96428571	1.93769922	1.80519956
THREONINE-DEG2-PWY	threonine degradation II	2	1	1.25911262	1.90509234
GLUCONSUPER-PWY	D-gluconate degradation	2	1	1.702271	2.3647267
PWY-66	GDP-L-fucose biosynthesis I (from GDP-D-mannose)	2	1	2.99269776	2.42917244
PWY0-661	PRPP biosynthesis II	2	1	2.88193561	1.72370551
PWY-6894	thiamin diphosphate biosynthesis I (E. coli)	2	1	2.70271621	2.35363775
PWY-7181	pyrimidine deoxyribonucleosides degradation	2	1	1.15009838	1.93460402
PWY0-1300	2-O-alpha-mannosyl-D-glycerate degradation	2	1	2.45899684	2.4412234
2PHENDEG-PWY	phenylethylamine degradation I	2	1	1.97359284	2.09844355
PWY0-1309	chitobiose degradation	2	1	1.88736692	1.19095321
TRESYN-PWY	trehalose biosynthesis I	2	1	1.83677266	3.00331018
PWY-7247	beta-D-glucuronide and D-glucuronate degradation	2	1	1.82541516	1.60708482
PWY-46	putrescine biosynthesis III	2	1	1.78260691	1.40424707
PWY-6019	pseudouridine degradation	2	1	3.23424124	2.69738572
XYLCAT-PWY	xylose degradation I	2	1	2.34239671	3.07625823
PWY0-1466	trehalose degradation VI (periplasmic)	2	1	1.70019343	4.27176029
PWY0-1477	ethanolamine utilization	2	1	2.32607631	1.9938891
GLUCARGALACTSUPER-PWY	superpathway of D-glucarate and D-galactarate degradation	5	1	1.85197625	1.98616611
AST-PWY	arginine degradation II (AST pathway)	5	1	1.67181348	2.15994831
GLUCARDEG-PWY	D-glucarate degradation I	4	1	1.69740595	1.84433906
GALACTARDEG-PWY	D-galactarate degradation I	4	1	1.69740595	1.89776655
PWY0-541	cyclopropane fatty acid (CFA) biosynthesis	1	NC	1.49596218	1.94296286

TREDEGLOW-PWY	trehalose degradation I (low osmolarity)	1	NC	2.18675062	1.41455366
PWY0-1315	L-lactaldehyde degradation (anaerobic)	1	NC	2.32846128	1.49622475
PWY-6476	cytidylyl molybdenum cofactor bio-synthesis	1	NC	2.73758113	6.40687046
TRYPDEG-PWY	tryptophan degradation II (via py-ruvate)	1	NC	2.71945032	2.32442325
PWY0-1306	L-galactonate degradation	1	NC	2.65064294	2.07270313
PWY0-1313	acetate conversion to acetyl-CoA	1	NC	1.19407481	4.21849854
PYRUVOX-PWY	pyruvate oxidation pathway	1	NC	1.1743514	3.66245495
PWY0-1527	curcumin degradation	1	NC	2.09016159	3.65971023
PWY-4621	arsenate detoxification II (glutaredoxin)	1	NC	1.39610105	1.14732764
SORBDEG-PWY	D-sorbitol degradation II	1	NC	1.25727254	1.08246131

Table S2. Pathways that are downregulated in both starvation and toxification. Pathway ID and name are according to EcoCyc database annotations, and normalized enrichment score is calculated using the R package fgsea.

Pathway ID	Name	Gene Set Size	Spearman correlation	Toxication NES	Starvation NES
PWY-6164	3-dehydroquinate biosynthesis I	4	0.2	-1.7170986	-1.6743143
1CMET2-PWY	formylTHF biosynthesis	13	0.21028159	-2.5127379	-2.2476814
PWY0-1544	proline to cytochrome bo oxidase electron transfer	5	0.3	-1.8036565	-2.0335072
PWY-7221	guanosine ribonucleotides de novo biosynthesis	4	0.4	-1.9758629	-1.7332184
PWY-6123	inosine-5'-phosphate biosynthesis I	5	0.4	-2.2939608	-2.0663072
SULFATE-CYS-PWY	superpathway of sulfate assimilation and cysteine biosynthesis	14	0.40468084	-1.8650526	-2.3251339
BRANCHED-CHAIN-AA-SYN-PWY	superpathway of leucine, valine, and isoleucine biosynthesis	16	0.54411886	-2.3907053	-2.3628305
VALSYN-PWY	valine biosynthesis	9	0.55064377	-1.9802507	-2.1931326
DAPLYSINESYN-PWY	lysine biosynthesis I	11	0.57028521	-2.1073292	-1.9758616
THRESYN-PWY	threonine biosynthesis	7	0.57659998	-2.1819213	-2.2058568
TRNA-CHARGING-PWY	tRNA charging	107	0.62366092	-4.4279593	-2.5551741
PEPTIDOGLYCANSYN-PWY	peptidoglycan biosynthesis I (meso-diaminopimelate containing)	17	0.68697631	-1.7201171	-1.9180572
DENOVOPURINE2-PWY	superpathway of purine nucleotides de novo biosynthesis II	21	0.68918484	-3.4673257	-2.8912608
PWY-6387	UDP-N-acetylmuramoyl-pentapeptide biosynthesis I (meso-DAP-containing)	9	0.69488131	-1.8992943	-1.8886918
PHESYN	phenylalanine biosynthesis I	5	0.7	-1.89207	-1.8678241
ECASYN-PWY	enterobacterial common antigen biosynthesis	11	0.7054586	-1.9152036	-2.1115153
LEUSYN-PWY	leucine biosynthesis	6	0.71428571	-2.1173865	-1.9587867
PRPP-PWY	superpathway of histidine, purine, and pyrimidine biosynthesis	43	0.72091986	-3.5866655	-3.2680707
PWY-6628	superpathway of phenylalanine biosynthesis	16	0.7363165	-2.4289374	-2.510254
ARO-PWY	chorismate biosynthesis I	11	0.73973495	-1.941385	-2.1526856
PWY0-781	aspartate superpathway	26	0.75367693	-2.6576584	-2.5798931
COMPLETE-ARO-PWY	superpathway of phenylalanine, tyrosine, and tryptophan biosynthesis	21	0.75932767	-2.6053657	-2.7188438
PWY0-1335	NADH to cytochrome bo oxidase electron transfer	17	0.76444213	-2.5689955	-2.4393504
PWY-6126	superpathway of adenosine nucleotides de novo biosynthesis II	9	0.76666667	-2.3916299	-1.97031
ALL-CHORISMATE-PWY	superpathway of chorismate metabolism	52	0.77022278	-2.8102534	-2.5571267
PWY-6629	superpathway of tryptophan biosynthesis	16	0.77309995	-2.2557452	-2.4093065
P4-PWY	superpathway of lysine, threonine and methionine biosynthesis I	20	0.79094258	-2.4644023	-2.3595712
PYRIDOXSYN-PWY	pyridoxal 5'-phosphate biosynthesis I	7	0.79282497	-1.992129	-1.9864921
TYRSYN	tyrosine biosynthesis I	4	0.8	-1.7577619	-1.6842574
PWY0-1329	succinate to cytochrome bo oxidase electron transfer	8	0.80511756	-1.9386191	-2.0145265
PWY0-1479	tRNA processing	8	0.80995314	-2.214798	-1.9543398

LPSSYN-PWY	superpathway of lipopolysaccharide biosynthesis	20	0.81108643	-2.2741008	-2.1287715
PWY0-845	superpathway of pyridoxal 5'-phosphate biosynthesis and salvage	9	0.8136762	-2.0845593	-2.0788978
MET-SAM-PWY	superpathway of S-adenosyl-L-methionine biosynthesis	11	0.83541781	-2.1197985	-2.0682583
METSYN-PWY	homoserine and methionine biosynthesis	10	0.83637445	-1.9654649	-2.0024894
PWY-6125	superpathway of guanosine nucleotides de novo biosynthesis II	9	0.84519568	-2.3505158	-1.8166431
KDO-NAGLIPASYN-PWY	superpathway of (KDO)2-lipid A biosynthesis	16	0.88141026	-2.3873531	-2.0658268
PWY-6277	superpathway of 5-aminoimidazole ribonucleotide biosynthesis	6	0.88571429	-2.481489	-2.2668217
PWY-6122	5-aminoimidazole ribonucleotide biosynthesis II	5	0.9	-2.2787075	-2.1128649
PWY-6121	5-aminoimidazole ribonucleotide biosynthesis I	5	0.9	-2.3204882	-2.1098019
PWY0-162	superpathway of pyrimidine ribonucleotides de novo biosynthesis	11	0.90545284	-2.313524	-2.0679254
GLUTAMINDEG-PWY	glutamine degradation I	9	0.91538573	-2.2115874	-1.9595464
PWY-5686	UMP biosynthesis	8	0.9187082	-2.0578243	-1.8682132
SER-GLYSYN-PWY	superpathway of serine and glycine biosynthesis I	6	0.94112395	-1.8912768	-1.769186
PWY-7343	UDP-glucose biosynthesis	2	1	-1.7850793	-1.699465
PWY-6605	adenine and adenosine salvage II	2	1	-1.9327137	-3.38289
HOMOSER-THRESYN-PWY	threonine biosynthesis from homoserine	2	1	-1.9119924	-3.4803336
MALATE-ASPARTATE-SHUTTLE-PWY	aspartate degradation II	2	1	-1.7983406	-3.8467327
PWY-5965	fatty acid biosynthesis initiation III	2	1	-1.4155951	-1.7037825
PWY-2161	folate polyglutamylation	2	1	-1.7341271	-3.3131773
PWY-901	methylglyoxal degradation II	2	1	-1.5556089	-1.6559264
PWY-4381	fatty acid biosynthesis initiation I	2	1	-1.7069039	-1.4797282
GLUTSYNIII-PWY	glutamate biosynthesis III	3	1	-1.8900618	-1.8192044
AMMASSIM-PWY	ammonia assimilation cycle III	3	1	-1.8571243	-1.8192044
PWY-7335	UDP-N-acetyl-alpha-D-mannosaminouronate biosynthesis	2	1	-1.4983814	-2.6058321
GLUTAMINEFUM-PWY	glutamine degradation II	2	1	-2.8905575	-4.8939616
PWY-7219	adenosine ribonucleotides de novo biosynthesis	3	1	-1.7681931	-1.7327185
GLUTSYN-PWY	glutamate biosynthesis I	2	1	-2.8905575	-4.8939616
THIOREDOX-PWY	thioredoxin pathway	1	NC	-1.651714	-3.7466738
ASPARTATESYN-PWY	aspartate biosynthesis	1	NC	-1.7983406	-3.8467327
GLYSYN-PWY	glycine biosynthesis I	1	NC	-2.9459969	-5.7535018
PWY-5785	di-trans,poly-cis-undecaprenyl phosphate biosynthesis	1	NC	-1.3916115	-2.277032
PWY0-662	PRPP biosynthesis I	1	NC	-2.9390604	-4.2513074
SAM-PWY	S-adenosyl-L-methionine biosynthesis	1	NC	-1.9408047	-2.4097819
PWY-6268	adenosylcobalamin salvage from cobalamin	1	NC	-1.1325597	-1.9376787
KDOSYN-PWY	KDO transfer to lipid IVA I	1	NC	-1.1913758	-1.2113179
PWY-6617	adenosine nucleotides degradation III	1	NC	-1.2055085	-1.717672

BSUBPOLYAMSYN-PWY	spermidine biosynthesis I	1	NC	-1.9988552	-3.7014181
GLNSYN-PWY	glutamine biosynthesis I	1	NC	-2.0239153	-4.9118033

Table S3. Pathways uniquely enriched in starvation. Pathway ID and name are according to EcoCyc database annotations, and normalized enrichment score is calculated using the R package fgsea.

Pathway ID	Name	Gene Set Size	Spearman correlation	Toxication NES	Starvation NES
FAO-PWY	fatty acid beta-oxidation I	9	-0.0666667	0	2.22387757
PWY-4261	glycerol degradation I	5	0.5	0	2.03254717
PWY0-1182	trehalose degradation II (trehalase)	3	0.5	0	1.62706335
PWY-6952	glycerophosphodiester degradation	6	0.71428571	0	1.79463742
PWY0-381	glycerol and glycerophosphodiester degradation	7	0.75678747	0	1.92648052
GLYOXDEG-PWY	glycolate and glyoxylate degradation II	5	0.9	0	1.93846673
PWY0-1299	arginine dependent acid resistance	2	1	0	1.19479501
DARABCAT-PWY	D-arabinose degradation II	1	NC	0	1.26124042
PWY-7346	UDP-alpha-D-glucuronate biosynthesis (from UDP-glucose)	1	NC	0	2.0622656
PWY0-1337	oleate beta-oxidation	1	NC	0	3.74727095
MANNIDEG-PWY	mannitol degradation I	1	NC	0	3.20579409
GLUAMCAT-PWY	N-acetylglucosamine degradation I	2	NC	0	1.21830745
PWY-7179	purine deoxyribonucleosides degradation	2	NC	0	1.39473893
PWY-6028	acetoin degradation	2	NC	0	1.47252358

Table S4. Pathways that are uniquely downregulated in starvation. Pathway ID and name are according to EcoCyc database annotations, and normalized enrichment score is calculated using the R package fgsea.

Pathway ID	Name	Gene Set Size	Spearman correlation	Toxication NES	Starvation NES
GLYCLEAV-PWY	glycine cleavage	4	-0.2108185	0	-1.7444687
BETSYN-PWY	glycine betaine biosynthesis I (Gram-negative bacteria)	2	-1	0	-1.5956464
PWYCQD-2	dTDP-N-acetylviosamine biosynthesis	6	0.13093073	0	-1.9469392
OANTIGEN-PWY-1	O-antigen building blocks biosynthesis (E. coli)	12	0.30623505	0	-2.2262838
GALACTMETAB-PWY	galactose degradation I (Leloir pathway)	5	0.3354102	0	-1.8345093
SO4ASSIM-PWY	sulfate reduction I (assimilatory)	6	0.3927922	0	-2.1430812
PYRUVDEHYD-PWY	pyruvate decarboxylation to acetyl CoA	3	0.5	0	-1.6142377
PWY-5084	2-oxoglutarate decarboxylation to succinyl-CoA	3	0.5	0	-1.6142377
PWY-7315	dTDP-N-acetylthomosamine biosynthesis	6	0.50709255	0	-1.8100348
PWY-7184	pyrimidine deoxyribonucleotides de novo biosynthesis I	8	0.54802458	0	-1.7702754
ILEUSYN-PWY	isoleucine biosynthesis I (from threonine)	10	0.65229728	0	-2.0483919
DTDPRHAMSYN-PWY	dTDP-L-rhamnose biosynthesis I	6	0.65465367	0	-1.9469392
HOMOSERSYN-PWY	homoserine biosynthesis	4	0.73786479	0	-1.6251729
TRPSYN-PWY	tryptophan biosynthesis	5	0.82078268	0	-1.7667447
ASPARAGINESYN-PWY	asparagine biosynthesis II	2	1	0	-1.9602794
PWY-6890	4-amino-2-methyl-5-diphosphomethylpyrimidine biosynthesis	2	1	0	-1.0344595
PWY0-1325	superpathway of asparagine biosynthesis	2	1	0	-1.9602794
PWY-6700	queuosine biosynthesis	4	1	0	-1.6297352
HISTSYN-PWY	histidine biosynthesis	9	NC	0	-2.2452096
PWY-7344	UDP-D-galactose biosynthesis	1	NC	0	-3.9647485
PWY0-1517	sedoheptulose bisphosphate bypass	2	NC	0	-2.3330402
PWY0-501	lipoate biosynthesis and incorporation I	2	NC	0	-1.1472346
GLUTATHIONESYN-PWY	glutathione biosynthesis	2	NC	0	-1.4696166
PWY0-1275	lipoate biosynthesis and incorporation II	2	NC	0	-1.3449008
PWY-6618	guanine and guanosine salvage III	1	NC	0	-1.4832385
PWY0-522	lipoate salvage I	1	NC	0	-1.3449008
SALVPURINE2-PWY	xanthine and xanthosine salvage	1	NC	0	-2.0936911
ASPARAGINE-BIOSYNTHESIS	asparagine biosynthesis I	1	NC	0	-2.1628747
GLUT-REDOX-PWY	glutathione redox reactions II	1	NC	0	-1.2122565
PWY0-1295	pyrimidine ribonucleosides degradation	2	NC	0	-1.4918647
PWY-5340	sulfate activation for sulfonation	3	NC	0	-1.6277355

Table S5. Pathways that are uniquely enriched in toxicity. Pathway ID and name are according to EcoCyc database annotations, and normalized enrichment score is calculated using the R package fgsea.

Pathway ID	Name	Gene Set Size	Spearman correlation	Toxicity NES	Starva-tion NES
PWYCQD-3	N-acetyl-galactosamine degradation	9	0.51666667	1.84151128	0
PWYCQD-4	galactosamine degradation	8	0.66666667	1.9179961	0
GALACTITOLCAT-PWY	galactitol degradation	5	0.7	1.59677363	0
PWY0-1321	nitrate reduction III (dissimilatory)	12	0.8041958	1.90376903	0
3-HYDROXYPHENYLACETATE-DEGRADATION-PWY	4-hydroxyphenylacetate degradation	8	0.88095238	1.73575101	0
PWY0-1356	formate to dimethyl sulfoxide electron transfer	9	0.88333333	1.69948976	0
PWY-6690	cinnamate and 3-hydroxycinnamate degradation to 2-oxopent-4-enoate	8	0.92857143	1.72900525	0
HCAMHPDEG-PWY	3-phenylpropanoate and 3-(3-hydroxyphenyl)propanoate degradation to 2-oxopent-4-enoate	8	0.92857143	1.72900525	0
PWY0-1277	3-phenylpropionate and 3-(3-hydroxyphenyl)propionate degradation	12	0.97022916	1.92679151	0
RHAMCAT-PWY	L-rhamnose degradation I	4	1	1.58032918	0
PWY0-1465	D-malate degradation	1	NC	1.36929171	0
PWY0-981	taurine degradation IV	1	NC	1.33115815	0

Table S6. Pathways that are uniquely downregulated in toxification condition. Pathway ID and name are consistent with EcoCyc database annotations, and normalized enrichment score is calculated with R package fgsea.

Pathway ID	Name	Gene Set Size	Spearman correlation	Toxication NES	Starvation NES
PWY-5188	tetrapyrrole biosynthesis I (from glutamate)	10	0	-2.1828993	0
PWY0-1061	superpathway of alanine biosynthesis	8	0.22094698	-1.8691385	0
PWY0-881	superpathway of fatty acid biosynthesis I (E. coli)	9	0.39167473	-2.4002279	0
PWY0-862	cis-dodecenoyl biosynthesis	5	0.46169026	-1.9822633	0
PWY-5989	stearate biosynthesis II (bacteria and plants)	5	0.46169026	-1.9764809	0
FASYN-ELONG-PWY	fatty acid elongation -- saturated	7	0.51887452	-2.1586643	0
PWY-5973	cis-vaccenate biosynthesis	7	0.52357031	-2.0937013	0
BIOTIN-BIOSYNTHESIS-PWY	biotin biosynthesis I	11	0.54067025	-1.7848757	0
PWY-5971	palmitate biosynthesis II (bacteria and plants)	6	0.5768179	-1.9822633	0
PWY-6284	superpathway of unsaturated fatty acids biosynthesis (E. coli)	8	0.59971229	-2.0838521	0
FASYN-INITIAL-PWY	superpathway of fatty acid biosynthesis initiation (E. coli)	4	0.63245553	-1.8415528	0
PWY0-163	salvage pathways of pyrimidine ribonucleotides	7	0.70418685	-1.8942574	0
ARGSYN-PWY	arginine biosynthesis I (via L-ornithine)	11	0.7723047	-1.7913983	0
PWY0-166	superpathway of pyrimidine deoxyribonucleotides de novo biosynthesis (E. coli)	12	0.80049837	-1.9230626	0
TCA	TCA cycle I (prokaryotic)	19	0.80158908	-1.7796264	0
PWY-7220	adenosine deoxyribonucleotides de novo biosynthesis II	6	0.94285714	-1.9280087	0
PWY-7222	guanosine deoxyribonucleotides de novo biosynthesis II	6	0.94285714	-1.9280087	0
GLUTDEG-PWY	glutamate degradation II	2	1	-1.7983406	0
PWY0-1534	hydrogen sulfide biosynthesis I	2	1	-1.7983406	0
PWY-5123	trans, trans-farnesyl diphosphate biosynthesis	2	1	-1.2644685	0
PWY0-1221	putrescine degradation II	4	1	-1.7084731	0
PWY0-1021	alanine biosynthesis III	2	NC	-1.8282391	0
ALANINE-SYN2-PWY	alanine biosynthesis II	2	NC	-1.0738934	0
PWY0-1433	tetrahydromonapterin biosynthesis	2	NC	-1.4665294	0
PWY-5783	octaprenyl diphosphate biosynthesis	1	NC	-1.1969374	0

Wang et al 45